THE ELASTIC SCATTERING OF PROTONS BY F^{19} AND N^{14}

Thesis by

Theodore S. Webb, Jr

In Partial Fulfillment of the Requirements

for the Degree of

Doctor of Philosophy

California Institute of Technology

Pasadena, California

1955

ACKNOWLEDGEMENTS

It is a pleasure to acknowledge the assistance and guidance of Professors W.A. Fowler, C.C. Lauritsen, T. Lauritsen, and C.A. Barnes during the course of these experiments. I am also indebted to Dr. E. Baranger and Professor R.F. Christy for numerous discussions regarding the theoretical aspects of these experiments and to Mr. F.B. Hagedorn for his assistance in performing much of the experimental work.

I wish to express my appreciation to the Dow Chemical Company and the International Business Machines Corporation for fellowships during the academic years 1953-1954 and 1954-1955, respectively.

These experiments were supported by the joint program of the Office of Naval Research and the Atomic Energy Commission.

ABSTRACT

The elastic scattering of protons by F^{19} and N^{14} has been investigated in the proton energy range 550 to 1800 kev. For $F^{19}(p,p)$ the differential cross section has been measured for proton energies from 550 to 1800 kev at center-of-mass angles of 90, 125.3, and 159.8 degrees and for proton energies from 1300 to 1500 kev at 53.2, 60, 70, 80, 100, 110, and 136 degrees. Pronounced scattering anomalies were observed near 669 (1^+), 843 (0^+), 873 (1^- or 2^-), 935 (1^+), 1346 (1^- or 2^-), 1372 (1^- or 2^-), 1422 (1^+), and 1700 kev. For $N^{14}(p,p)$ the cross section has been measured from 600 to 1800 kev at 154 degrees and from 1.0 to 1.1 and 1.4 to 1.8 Mev at 90 and 125.3 degrees. Anomalies were observed near 1.06 ($1/2^+$ or $3/2^+$), 1.55 ($1/2^+$), 1.73 ($3/2^-$ or $5/2^-$), and 1.79 ($3/2^-$ or $5/2^-$) Mev. The indicated spin and parity assignments are required by the results of these experiments. The relative stopping cross section for protons in LiF has been measured for proton energies from 400 to 1600 kev, and experimental and theoretical investigations of the effects of finite energy resolution on observed cross sections have been made.

TABLE OF CONTENTS

I. INTRODUCTION

The study of the elastic scattering of protons by a given nucleus is of particular interest in connection with the information which it may yield concerning the excited states in the compound nucleus formed in the reaction. Such excited states will, in general, give rise to pronounced variations of the scattering from the classical Rutherford law, and the analysis of these anomalies may frequently be used to infer certain properties of the excited states involved. Among the interesting characteristics of nuclear levels are the excitation energy, width, partial widths or probabilities for various modes of decay, total angular momentum, parity, relative angular momentum of the particles forming the state, and isotopic spin. In general, the elastic scattering alone will not allow the determination of all these quantities but may be used in conjunction with other measurements for their determination.

The analysis of the elastic scattering measurements involves the comparison of the observed scattering with that calculated for various values of these parameters. In making these comparisons, however, complications sometimes arise as a result of the finite energy resolution of the experiment, since the anomalies frequently occur as rapid variations in the scattering as a function of the proton energy. In order to evaluate these effects, certain experimental and theoretical investigations of energy resolution have been made in connection with the present experiments.

In addition to the interest, per se, in the levels of Ne^{20} and O^{15}, both $F^{19}(p,p)$ and $N^{14}(p,p)$ are of interest in other connections. The former, in relation to the recent investigations of the two low lying levels in F^{19} at 109 and 196 kev by the study of $F^{19}(p,p')$; and the latter, in relation to the low energy cross section for $N^{14}(p,\gamma)$ which is of considerable interest in the study of stellar energy production.

In the case of the bombardment of F^{19} by protons in the present energy range, several reactions occur in addition to $F^{19}(p,p)$: $F^{19}(p,p'\gamma)$, $F^{19}(p,\alpha)$, $F^{19}(p,\alpha\gamma)$, $F^{19}(p,\alpha\pi)$, and $F^{19}(p,\gamma)Ne^{20}$. The (p,α) reactions have been extensively studied by many investigators[1], and $F^{19}(p,p')$ has recently been studied by Barnes[2] and Peterson, et. al.[3] at this Laboratory. Several resonances in $F^{19}(p,\gamma)$ have been observed, but the probability of this reaction is quite small in all cases. In addition to the present work, the elastic scattering has recently been investigated by Dearnaley[4].

From the investigations of the various reactions listed above, excitation energies and total widths for a considerable number of levels in Ne^{20} in the energy range of the present experiment are known. For several of these levels spin, parity and proton angular momentum are also known from these reactions, and for most of the others many combinations of these quantities can be excluded. In addition, the measured cross sections for $F^{19}(p,\alpha)$ and $F^{19}(p,p')$ allow the division of the total width, Γ, into the partial width for the emission of protons, Γ_p, and the reaction width, $\Gamma_\alpha + \Gamma_{p'}$, in only two ways for a given spin assignment. With this information already available it was believed that the elastic scattering study

would be of considerable value in completing the determination of the parameters of many of these levels.

In the course of this investigation it was found necessary to determine the stopping cross sections for protons in lithium fluoride, and a measurement of the relative values of this quantity was made for proton energies from 400 to 1600 kev.

For N^{14} + p, the situation is simplified considerably by the absence of other particle reactions, since only $N^{14}(p,p)$ and $N^{14}(p,\gamma)\ O^{15}$ are energetically possible in the present range of proton bombarding energies. The latter reaction was studied by Duncan and Perry[5], who determined excitation energies and widths for five levels in the present energy range. The elastic scattering for proton energies above 1 Mev has also been recently observed by Gove, et. al.[6] and Tautfest, et. al.[7]

II. EXPERIMENTAL APPARATUS

1. General

Protons for these experiments were obtained from the 2.0 Mv electrostatic generator of this Laboratory which was constructed in 1938[8] and partially rebuilt in 1946 and 1952.[9] The proton beam was analyzed by an 80 degree electrostatic analyzer of 1 meter radius and 1 mm entrance and exit slits which was built for use with the magnetic spectrometer. The design of the analyzer is similar to the 90 degree analyzer described by Fowler, et.al.[10] The incident beam was monitored by integration of the charge striking the target, and the scattered protons were analyzed by a double focussing magnetic spectrometer which is mounted to allow a continuously variable scattering angle from 0 to 160 degrees with respect to the incident beam direction.[11] The scattered protons were detected by means of a zinc sulphide screen or a cesium iodide crystal placed at the exit slit of the spectrometer. A schematic representation of the experimental arrangement is given in Figures 1A and 1B.

2. Calibration of the apparatus

The calibrations which are necessary for experiments of this type are the energy calibration of the electrostatic analyzer and magnetic spectrometer, and the determination of the effective solid angle of the magnetic spectrometer.

The electrostatic analyzer may be conveniently calibrated by observing the thick target gamma ray yield over a proton energy range containing a known resonance of small width. When a thick target is used for observing the particle reaction, this procedure permits calibration of the analyzer at the same time the reaction is being observed, and the method does not require a separate determination of the target thickness as required in a thin target energy calibration. In the thick target gamma ray yield, the mid-point of the observed step occurs at the resonance energy, E_R. If we designate the incident proton energy by E_{10}, the thickness of any contamination layer on the target surface by ΔE_1 (in energy units at energy E_{10}), and the electrostatic analyzer setting (proportional to the voltage on the analyzer plates) by S_R, we have to first order:[12]

$$E_{10} = zC_e S_R \left(1 + \frac{E_{10}}{2Mc^2}\right) . \qquad (1)$$

C_e is the constant of the analyzer to be determined, M is the proton rest mass, and c is the velocity of light. The reaction energy in the surface layer of the target will then be $E_{10} - \Delta E_1 - zeV_T$, where V_T is the potential of the target with respect to the equilibrium orbit of the analyzer, and ze is the charge of the bombarding particle. We observe the mid-point of the step in the gamma ray curve at an analyzer setting S_R where :

$$E_{10} = E_R + \Delta E_1 + zeV_T = zC_e S_R \left(1 + \frac{E_{10}}{2Mc^2}\right) \qquad (2)$$

Thus to first order terms:

$$C_e = \frac{E_R}{zS_R}\left(1 + \frac{zeV_T + \Delta E_1}{E_R} - \frac{E_R}{2Mc^2}\right) \quad . \qquad (3)$$

In the present experiment the gamma resonances in $F^{19}(p,\alpha\gamma)$ at 873.5 and 1372 kev were used to calibrate the electrostatic analyzer by this procedure.

After calibrating the electrostatic analyzer it is then possible to calibrate the energy scale of the magnetic spectrometer at any convenient bombarding energy, E_{10}, by observing the elastic scattering at a known angle, θ, from a target of known atomic mass, usually copper in these experiments. If the fluxmeter setting for the spectrometer (inversely proportional to the magnetic field in the type used) is I, then the acceptance energy of the spectrometer, E_{20}, is to first order:[12]

$$E_{20} = \frac{z^2 C_m}{MI^2}\left(1 - \frac{E_{20}}{2Mc^2}\right) \quad , \qquad (4)$$

where C_m is to be determined. The mid-point in the rise of the momentum spectrum of the scattered particles (obtained by varying the spectrometer setting with the bombarding energy fixed) corresponds to the energy of particles scattered from the front surface of the target, except for a correction due to the resolution which is usually negligible.[12] This scattering takes place at an energy, $E_{10} - \Delta E_1 - zeV_T$, and the energy after scattering is $k(E_{10} - \Delta E_1 - zeV_T)$ where k is given in equation (10). For the usual target arrangement (the target surface making equal angles with the incident beam direction and the

direction of scattering) these particles will reach the spectrometer with an energy E_{20}, where:

$$E_{20} = k\left(E_{10} - \Delta E_1 - zeV_T\right) - \frac{\epsilon_2}{\epsilon_1}\,\Delta E_1 + zeV_T \qquad (5)$$

ϵ_1 and ϵ_2 are the stopping cross sections for the particles in the contamination layer at energies E_{10} and E_{20}, respectively. Thus we have from (4):

$$C_m = \frac{Mk}{z^2} E_{10} I^2 \left[1 - \frac{\epsilon_2 + k\,\epsilon_1}{k\,\epsilon_1}\,\frac{\Delta E_1}{E_{10}} + \frac{1 - k}{k}\,\frac{zeV_T}{E_{10}} + \frac{kE_{10}}{2Mc^2}\right] \qquad (6)$$

where I is the magnetometer setting at the mid-point of the rise in the momentum spectrum of the scattered particles.

Having determined C_e and C_m the effective solid angle is then found by observing the yield of scattered particles from a target for which the scattering cross section is known. In the present experiments copper targets were used and Rutherford scattering was assumed. From this yield the ratio of the solid angle (including counter efficiency) to the spectrometer resolution can be found from equation (17).

The primary uncertainty in the energy calibration is due to the presence of contamination layers, ΔE_1. The most effective method of avoiding this difficulty is, of course, the use of clean targets which do not become contaminated rapidly. In many cases this is not possible, however, and some correction must be made for contamination. By repeating the observation of the gamma ray or momentum profile several times on the same target it is often possible to determine the rate of contamination and to extrapolate to zero bombardment, or to affirm that contamination

is negligible. In some cases it is possible to observe the scattering peak due to the contaminants (which are usually carbon and oxygen), and to determine thethickness from this. Where the layer is appreciable, the magnetic spectrometer may be used to determine the thickness by observing the shift in the mid-point of the momentum profile, although this method is generally uncertain to 1-2 kev.

To evaluate ΔE_1 by the latter method, we observe the momentum profile of particles elastically scattered from the target in question, and those elastically scattered from a clean target of, for example, copper at the same bombarding energy. If we denote the energy corresponding to the mid-point of the rise in the momentum spectrum by E_C and E_T for copper and the target in question respectively, and the bombarding energy in both cases by E_{10}, we have:

$$E_C = k_C \left[E_{10} - zeV_T\right] + zeV_T$$

$$E_T = k_T \left[E_{10} - zeV_T - \Delta E_1\right] - \frac{\epsilon_2}{\epsilon_1} \Delta E_1 + zeV_T \qquad (7)$$

If I_C and I_T are the magnetometer settings corresponding to E_C and E_T respectively, we obtain from (4) and (7):

$$\Delta E_1 = \frac{k_T \epsilon_1 E_{10}}{k_T \epsilon_1 + \epsilon_2} \left(1 - \frac{k_C I_C^2}{k_T I_T^2} - (k_C - k_T)\left(\frac{E_{10}}{2Mc^2} - \frac{zeV_T}{k_C k_T E_{10}}\right)\right) \qquad (8)$$

where E_{10} may be found to sufficient accuracy by neglecting the small terms in (1) and (3).

3. Target Preparation

The selection of satisfactory target materials and the preparation of targets frequently present a considerable problem in experiments of the present type. The experimental procedure for thick targets involves the use of the magnetic spectrometer to observe the scattered particles in a given momentum interval, corresponding to scattering in a given thin lamina of the thick target. If the target contains nuclei heavier than those from which the scattering is to be studied, this momentum interval will also contain particles scattered from the heavier species, the scattering occurring in a deeper lamina. This will, in general, produce a background yield comparable to the yield which is to be observed and the arrangement is therefore undesirable. If lighter elements only are present in the target it is usually possible to make observations in a momentum interval where it is kinematically impossible to have particles scattered from the extraneous nuclei. Thus an important criterion for a target material is that it contain only elements of lighter mass than that desired. In the case of fluorine this condition is easily met by lithium fluoride (LiF) which occurs as a white solid at room temperature and is readily available.

The most satisfactory method of target preparation for such work is by evaporation of the desired material on a suitable backing. The use of evaporated targets is desirable since the evaporation can be carried out in the evacuated target chamber immediately prior to use, thus avoiding contact with the air and

possible contamination. The mirror target surfaces resulting from evaporation are also desirable. Several attempts to produce satisfactory evaporated LiF targets on copper were made, but in every case the LiF layer was found to chip after a small amount of bombardment if the layer was thicker than a few kev. For this reason use was made throughout most of the experiment of pressed LiF pellets, although later considerations of energy resolution led to the evaporation of LiF on beryllium, and it was found that these targets were quite stable regardless of thickness.

For the preparation of the pressed LiF targets, copper plates $1\frac{1}{2}$" by $\frac{1}{2}$" by 1/16" with two 3/8" holes 1/32" deep inset in one face were used. The LiF powder was pressed into the holes using a highly polished steel press. This resulted in relatively smooth target surfaces which would reflect light at large angles. The behavior of the pressed targets was, in general, satisfactory although new targets spots frequently gave high and erratic yields for the first one or two bombardments. This effect was probably due to difficulty in charge collection caused by the insulating nature of the target material before bombardment, although it could also have been caused by the loss of fluorine from the target due to an initial fluorine excess or decomposition of LiF in the surface layers. As the effect was usually small (5-10%) and not reproducible, the equilibrium values of the yield, which were reached after a few microcoulombs of bombardment, were used. In addition to this rapid change a slow, reproducible decrease in yield with bombardment was also observed. This was probably

due to the dilution of the surface layer of the target by carbon and oxygen deposited during bombardment or, possibly, due to the decomposition of lithium fluoride and subsequent escape of fluorine from the target. By frequently changing to fresh target spots the size of this effect was kept below about five percent, and corrections were made for it by linear extrapolation to zero bombardment. Attempts were made to improve the behavior of the targets by heating the LiF before preparing them, but no noticeable improvement resulted from this treatment. The targets exhibited rapid discoloration on bombardment and would occasionally chip after long use.

The preparation of targets for the nitrogen experiment presented considerably more difficult problems. Among the compounds of nitrogen which satisfy the basic criterion discussed above are ammonia (NH_3), lithium nitride (Li_2N), beryllium nitride (Be_3N_2), boron nitride (BN), and melamine ($C_3N_6H_6$). Of these the latter two are not applicable to observations at scattering angles much smaller than 125 degrees since the energy difference between protons scattered from nitrogen and carbon or boron approaches the energy resolution of the magnetic spectrometer at those angles. Of the remaining materials, Li_2N is extremely unstable to decomposition under the action of water and several attempts to obtain evaporated and pressed targets of Li_2N failed, the evaporated targets containing only lithium and the pressed targets, lithium and oxygen. No nitrogen was found in any of these targets although a definite odor of ammonia resulted when the Li_2N was placed in water.

Considerable investigation of the use of ammonia targets was made since they would be applicable to forward angle scattering without difficulty. The procedure was to condense ammonia on a hollow tube filled with liquid nitrogen, the tube being mounted to rotate continuously during bombardment to reduce the amount of bombardment per unit area suffered by the target. Even with this precaution, however, the targets were rather unsatisfactory. The use of the cooled target surface greatly increased the surface contamination normally encountered, and the rapid contamination was probably the major factor in the poor target behavior which manifested itself as a rapid decrease in yield with bombardment. This effect gave, at best, a decrease of several percent after one hundred microcoulombs of bombardment. In addition, the yield from fresh target spots frequently varied by several percent and it was therefore necessary to check some reference point with each new target spot in regions where the cross section was changing rapidly. Excitation curves could be obtained only by taking few counts at each energy or by constantly changing to new spots and checking reference points to obtain relative values.

The remaining target material, Be_3N_2, has also been extensively investigated and found to present problems comparable to those encountered with ammonia. Be_3N_2 decomposes at a temperature slightly above its melting point and for this reason pressed targets had to be used. Individual targets were quite stable and gave reproducible results over long periods; different targets, however, were found to vary in yield over a range of about 20 percent. This was probably connected with the purity of the material

and the exact method of target preparation and handling since Be_3N_2 reacts fairly readily with water and appreciable oxygen was always observed with these targets, apparently distributed throughout the target material. In addition, the reaction products from Be + p gave an appreciable background, although most of the work was done using a cesium iodide detector which permitted most of these pulses to be biased out. Finally, the presence of beryllium makes the target material unsuitable for use at forward angles for the reasons described above. At 90 degrees there is sufficient separation in energy to resolve the protons scattered from the nitrogen and beryllium, although carbon and oxygen contamination complicated the observations at this angle.

In addition to the thick targets which have been investigated, considerable use has also been made of a thin target prepared by the bombardment of a beryllium disk by 25 kev nitrogen ions using the arrangement constructed by Mr. F.B. Hagedorn. The primary disadvantages in the use of thin targets is the need to make an additional determination of the absolute cross section or the target thickness and the greater time required for making observations, since the cross section in this case depends on the yield integrated over all energies. In the present case some difficulty was also encountered due to extensive carbon and oxygen contamination. This was unimportant at the larger scattering angles but presented a considerable problem at 90 degrees and made observations at forward angles impossible. The advantages in the use of thin targets in this case were the greater target

stability and the large increase in the overall energy resolution of the experiment (see Section VI).

III. EXPERIMENTAL PROCEDURE

In the present experiments we are interested in obtaining the scattering cross section per unit solid angle as a function of the bombarding proton energy immediately before scattering. This cross section is defined as

$$\frac{d\sigma}{d\Omega} = \frac{Y(E_1)}{N_B(E_1)N_T\Omega} \tag{9}$$

where $Y(E_1)$ is the number of particles scattered into the solid angle Ω for $N_B(E_1)$ bombarding particles with energy E_1 immediately before scattering, and N_T is the number of scattering nuclei per unit area perpendicular to the incident beam direction.

1. Thick Target Experiments

If charged particles of a given energy, E_{10}, are incident on a thick target, the momentum spectrum of the elastically scattered particles will display a sudden step at a momentum corresponding to an energy kE_{10}, where k depends only on the angle of observation and the masses of the bombarding particle and the target nuclei and is determined from the conservation of energy and momentum:[12]

$$k^{1/2} = \left(\frac{\partial E_2}{\partial E_1}\right)^{1/2} = \frac{M_1}{M_o + M_1}\cos\theta + \left[M_o^2 - M_1^2\sin^2\theta\right]^{1/2}\frac{1}{M_o + M_1} \tag{10}$$

In this expression M_1 and M_o refer to the incident particles and the target nuclei, respectively, and θ is the laboratory

angle of scattering with respect to the incident beam direction. (It should be noted that (10) is valid only for elastic scattering). This step in the momentum spectrum corresponds to particles scattered in the surface layer of the target which have suffered no energy loss in passing through the target material. At any energy of observation less than kE_{10} the observed particles are those scattered from a layer of the target behind the surface which have suffered energy losses in passing through the target material before and after scattering. The depth at which the scattering takes place is determined by the energies of the bombarding and scattered particles as described below, and the thickness of the lamina in which the scattering occurs is determined by the resolution or energy acceptance interval of the spectrometer with which the particles are observed. By adjusting these quantities we are therefore able to observe the scattering which occurs at a given depth in the target from a lamina of given thickness.

The shape of the momentum profile of the scattered particles, especially as regards the sharpness of the rise, indicates the target surface condition and contamination and represents a critical criterion in determining the suitability of a given target, excessive rounding off of the top or bottom of the step being the usual manifestation of defects. Figure 2 shows several typical profiles for the targets used in the present experiments.

After examining the momentum spectrum from the target, the procedure is to select a point on the profile, $E_{20} < kE_{10}$, where the full height of the rise obtains. Energy resolution con-

siderations suggest that $kE_{10} - E_{20}$ be as small as possible, but target wear, which manifests itself as a rounding off of the top of the step, puts a limit on the size of this quantity. Generally we have used $kE_{10} - E_{20}$ about one percent of E_{10} in the present experiments. The point E_{20} is designated as the "following point", and as the bombarding energy is varied the spectrometer acceptance energy is also varied so as to keep $(kE_{10} - E_{20})/ E_{10}$ constant.

With these considerations we may now proceed to evaluate the quantities appearing in equation (9) in terms of the quantities which are observed. We treat here only the case of elastic scattering; applications to the more general case are given by Milne[9], Warters,[11] and Brown, et. al. [12]. We assume that the thick target is homogeneous, that it presents a smooth surface to the incident particles, and that the normal to the target surface makes an angle θ_1 with respect to the incident beam direction and an angle θ_2 with respect to the angle of observation (see Figure 3). Then at any depth, t, in the target the energy of the incident beam will be

$$E_1 = E_{10} - \frac{\epsilon_1 nt}{\cos \theta_1} \quad , \tag{11}$$

where n is the number of target nuclei per unit volume and ϵ_1 is the average stopping cross section per target nucleus for the incident particles between energies E_{10} and E_1. If the scattering occurs at this depth, then the energy immediately after scattering is:

$$E_2 = kE_1 = k\left[E_{10} - \frac{\epsilon_1 nt}{\cos \theta_1}\right] \tag{12}$$

The scattered particle will suffer an additional energy loss in leaving the target and will emerge from the target with energy E_{20}, where:

$$E_{20} = E_2 - \frac{\epsilon_2 nt}{\cos\theta_2} \quad . \tag{13}$$

ϵ_2 is the average stopping cross section per target nucleus between energies E_2 and E_{20}. Thus, the scattering energy may be found from (11) and (12) to be:

$$E_1 = \frac{E_{20} + \eta E_{10}}{k + \eta} = \frac{E_{20} + \eta E_{10}}{\epsilon_{eff}} \epsilon_1, \tag{14}$$

where $\eta = \frac{\epsilon_2 \cos\theta_1}{\epsilon_1 \cos\theta_2}$. Since the distribution of the energy E_1 is essentially continuous, we must observe the yield from a small range of energies δE_1 about E_1. The determination of δE_1 is made by the resolution of the spectrometer. Thus, $\delta E_1 = \frac{\epsilon_1 \delta E_{20}}{\epsilon_{eff}}$ and $\delta E_{20} = \frac{2E_{20}}{R_c}$ where $R_c = 2(1 + M) \frac{r_o}{\delta r_c}$. In these expressions, R_c is the momentum resolution, M is the magnification, r_o is the radius of the equilibrium orbit, and δr_c is the width of the exit window of the spectrometer.[12] Thus, we have:

$$\delta E_1 = \frac{\epsilon_1}{\epsilon_{eff}} \frac{2}{R_c} E_{20} \, . \tag{15}$$

The values of the quantities appearing in equation (9) for an incident energy E_{10}, and a spectrometer energy E_{20} may now be obtained. The yield, $Y(E_1)$, will be the number of particles detected for these settings for an integrated beam current, q. $N_b = \frac{q}{e}$,

where e is the electronic charge. The number of target nuclei per unit area which contribute to the observed scattering is given by:

$$N_T = \frac{\delta E_1}{\epsilon_1} = \frac{2E_{20}}{R_c \epsilon_{eff}} \tag{16}$$

Thus, substituting in equation (9), we have,

$$\frac{d\sigma}{d\Omega} = \frac{eYR_c \epsilon_{eff}}{2qE_{20}\Omega} = 8.011 \frac{YR_c \epsilon_{eff}}{\Omega q E_{20}} \times 10^{-5} \text{barns/steradian} \tag{17}$$

where Ω (in steradians) may be expressed in either the laboratory or the center-of-mass systems. Of the quantities appearing in this expression Y, E_{20}, and q are directly measured in the experiment, and the ratio R_c/q is obtained as described in Section II. The stopping cross section must be obtained independently.

The relation between the solid angles in the center-of-mass and laboratory systems is given by Brown, et. al.[12] as,

$$\frac{\Omega_c}{\Omega_L} \cong \frac{d\Omega_c}{d\Omega_L} = \frac{\left[(1 - \alpha^2 \sin^2\theta)^{1/2} + \alpha \cos\theta\right]^2}{\left[1 - \alpha^2 \sin^2\theta\right]^{1/2}}, \tag{18}$$

where θ is the laboratory angle of scattering and, for elastic scattering, $\alpha = M_1/M_o$. It is often of interest to convert laboratory angles into center-of-mass angles and vice versa; convenient expressions are:

$$\cos\theta_c = \cos\theta(1 - \alpha^2 \sin^2\theta)^{1/2} - \alpha \sin^2\theta$$

$$\tan\theta = \frac{\tan\theta_c}{1 + \alpha \sec\theta_c} \tag{19}$$

2. Thin Target Experiments

To obtain the expression for the cross section in terms of the observed quantities in a thin target experiment, we consider a target of thickness, t, parallel to the incident beam and denote by n(x) the number of target nuclei per unit volume at a depth x. The number of particles scattered into the solid angle Ω from a layer of width dx is then, from (9),

$$\frac{dN(x)}{dx}\,dx = \frac{dN(E_{20})}{dE_{20}}\,dE_{20} = \frac{d\sigma(E_1)}{d\Omega}\,n(x)N_B\Omega\,dx\ , \tag{20}$$

where E_1 is the energy of the incident beam at the depth x. Integrating both sides of equation (20) from x = 0 to x = t, we obtain

$$\frac{d\sigma}{d\Omega}\,nt\Omega\,N_B = \int_{x=o}^{x=t} dN(x) = \int_{x=o}^{x=t} \frac{dN(E_{20})}{dE_{20}}\,dE_{20}\ , \tag{21}$$

where $\frac{d\sigma}{d\Omega}$ is the average cross section over the energy interval E_{10} to $E_{10} + \epsilon_1 nt$, and n is the effective number of target nuclei per unit volume. If we now denote by $P(I,E_{20})$ the probability of detecting a particle of energy between E_{20} and $E_{20} + dE_{20}$ at a spectrometer setting I, the observed yield at this setting will be:

$$Y(I) = \int_o^\infty \frac{dN}{dE_{20}}\,P(I,E_{20})dE_{20}\ . \tag{22}$$

For the magnetic spectrometer used $P(I, E_{20})$ is approximately a square window of width (in units of I), $\Delta I = I_o / R_c$, centered at

$E_{20} = C_m / I_o^2$. Thus, dividing both sides of (23) by I and integrating from I = 0 to I = ∞, we have,

$$\int_o^\infty \frac{Y(I)}{I}\, dI = \int_o^\infty \ln \frac{I_o + \Delta I/2}{I_o - \Delta I/2} \frac{dN}{dE_{20}}\, dE_{20} \qquad (23)$$

or :

$$\int_o^\infty \frac{Y(I)}{I}\, dI = \frac{1}{R_c} \int_o^\infty \frac{dN}{dE_{20}}\, dE_{20} + O\left(\frac{1}{R_c^3}\right). \qquad (24)$$

Combining equations (21) and (24), we have,

$$\frac{d\sigma}{d\Omega} = \frac{R_c}{nt\Omega N_b} \int \frac{Y(I)}{I}\, dI = 1.602 \frac{R_c}{\Omega q} \frac{10^{11}}{nt} \int \frac{Y(I)}{I}\, dI \qquad (25)$$

in the notation of equation (17).

To obtain the quantities appearing in this equation, complete momentum profiles were observed at several energies and angles and the integral in (25) evaluated numerically. From these results relative cross sections were obtained for all the thin target experiments and these were normalized to the absolute cross sections determined from the thick target measurements. The profiles used are shown in Figures 4 and 5.

Excitation curves were obtained by observing the maximum yield from the nitrogen peak at each energy. These results were then converted to cross sections by determining the ratio of the maximum yield to the cross section at the various reference points and using these values to obtain the cross sections at intermediate energies. A more detailed description of the procedure is given in Section V.

IV. $F^{19}(p,p)$

1. Experimental Results

The results of the F^{19} investigations are presented in Figures 6 to 11 as the ratio of the observed cross section to Rutherford cross section. The Rutherford differential cross section can be written as:

$$\frac{d\sigma_R}{d\Omega_C} = 1.296 \left[\frac{Z_1 Z_o}{E_1} \frac{M_1 + M_o}{M_o} \csc^2 \frac{\theta_C}{2}\right]^2 \times 10^{-3} \text{ barns/steradian} \quad (26)$$

$$\frac{d\sigma_R}{d\Omega_L} = 1.296 \left(\frac{Z_1 Z_o}{E_1}\right)^2 \left[\csc^4 \frac{\theta_L}{2} - 2\left(\frac{M_1}{M_o}\right)^2 + 0\left(\frac{M_1}{M_o}\right)^4\right] \times 10^{-3} \text{ barns/ster.} \quad (27)$$

$$\frac{d\sigma_R}{d\Omega_C} = 0.1164 \left(\frac{1}{E_1}\right)^2 \csc^4 \frac{\theta_C}{2} \text{ barns/steradian} \quad (28)$$

In these expressions E_1, Z_1, and M_1 are the energy (in the laboratory system), charge, and mass respectively of the incident particle, and Z_o and M_o refer to the target nucleus. The subscripts C and L designate measurements in the center-of-mass and laboratory systems respectively.

The cross section was measured at center-of-mass angles of 90, 125.3 and 159.8 degrees for proton energies from 550 to 1800 kev and at angles of 53.2 60, 70, 80, 100, 110 and 136 degrees for proton energies from 1300 to 1500 kev. Pronounced anomalies were observed which are identified with known levels[1] of Ne^{20} at proton energies of 669, 843, 873, 935, 1346, 1372

and 1422 kev; in addition, a broad structure was observed in the region near 1700 kev which could be associated with one or more reported levels[1],[2] in this region. There also appear to be small, unresolved structures in the cross section corresponding to known resonances[1] at 900, 1092, and 1137 kev. Some investigations have also been made in the regions near 340 and 480 kev in an attempt to observe anomalies corresponding to reported resonances[1] at these energies. Target deterioration and carbon contamination caused a much greater decrease in yield with bombardment than at higher energies, however, and therefore no attempt to determine absolute cross sections was made. No anomaly greater than 20 percent of the Rutherford cross section was detected in either case, however.

The major uncertainty in the quoted cross sections is due to the uncertainty in the value of the LiF stopping cross section (the determination of the stopping cross section is discussed in the appendix) which is estimated to be about 5 percent. The probable error in the solid angle (involving the ratio of the cross section for elastic scattering to the stopping cross section for protons for copper) is taken to be 3 percent although recent investigations at this Laboratory by F.S.Mozer indicate the possibility of a systematic error of 5 - 10 percent in the solid angle determination. This effect is related to the copper targets used for the solid angle calibrations and would lower the quoted cross sections. The uncertainty due to target composition and behavior, estimated from the agreement of results from different targets, is about three percent. This gives a probable error in the absolute

values of about 7 percent. In addition, the irregularity of the target surface implied by the energy resolution of the experiment (see Section VI.) could introduce a systematic error in the cross section values. Rough estimates of this effect indicate that it is negligible at scattering angles larger than 90 degrees but that it could increase the observed yield by 5 to 10 percent at 60 degrees.

The uncertainty in the relative values of the cross section is about 5 percent arising from the uncertainty in the relative stopping cross section (4 percent) and the possible variation in the effective solid angle with energy and angle (3 percent). The statistical uncertainty of each point is less than 2 percent, and the current integrator reproducibility is about one percent.

2. Discussion

An analysis of these experimental results has previously been given by E. Baranger[15] who discusses the approximation involved in the theoretical expressions on which the present treatment is based.

The non-resonant scattering observed in this experiment can be fitted by considering only s-wave phase shifts, and it is therefore assumed that the higher non-resonant phase shifts are zero over the present energy range. For this assumption the elastic scattering cross section in the vicinity of a resonance of spin J formed by s-wave protons can be written as:[15]

$$\frac{\sigma}{\sigma_R} = 1 - \frac{2J+1}{2k\,\sigma_R^{1/2}} \left[\frac{\Gamma_p}{\Gamma} \sin\delta_J \cos\left(\delta_J + \theta_o + 2\varphi_J\right) + \sin\varphi_J \cos\left(\theta_o + \varphi_J\right)\right] + \frac{2J+1}{4k^2\,\sigma_R} \left[\left(\frac{\Gamma_p}{\Gamma} \sin\delta_J\right)^2 + \sin^2\varphi_J + 2\frac{\Gamma_p}{\Gamma} \sin\delta_J \sin\varphi_J \cos\left(\varphi_J + \delta_J\right)\right] \qquad (29)$$

For a resonance formed by higher orbital angular momentum, the expression is:[15]

$$\frac{\sigma}{\sigma_R} = 1 - \frac{2J+1}{2k\,\sigma_R^{1/2}} \left[\frac{\Gamma_p}{\Gamma} \sin\delta_J \cos\left(\theta_\ell + \delta_J\right) P_\ell(\cos\theta)\right] + \pi \frac{2\ell+1}{k^2\,\sigma_R} \left[\frac{\Gamma_p}{\Gamma} \sin\delta_J\right]^2 \sum_{m,M,T,R} \left[\alpha_R^{\,2}\alpha_T^{\,2} \left| Y_\ell^M(\theta,\varphi)\right|^2 \times \left|C_{R\ell}(J,M;M,0)\, C_{T\ell}(J,M;M-m,m)\right|^2\right] \qquad (30)$$

In these expressions k is the wave number, σ_R is the Rutherford cross section, Γ_p/Γ is the ratio of the proton width to the total width, δ_J is the resonance phase shift such that

$\delta_J = -\,\mathrm{ctn}^{-1}\,\frac{E - E_R}{\Gamma/2}$, φ_J is the non-resonant s-wave phase shift, θ_o and θ_ℓ are coulomb phase shifts such that

$$\theta_o = \frac{Ze^2}{\hbar v}\, \ln \sin^2\frac{\theta_c}{2}\,; \quad \theta_\ell = \theta_o + 2\sum_{n=1}^{\ell} \tan^{-1}\frac{\alpha}{n},$$

$Y_\ell^M(\theta,\varphi)$ is a spherical harmonic, $P_\ell(\cos\theta)$ is a Legendre

polynomial, and α_R and α_T are channel spin ratios such that $\sum_R \alpha_R^2 = 1$. For the case of $\ell \neq 0$, the cross section will also contain the non-resonant contribution of the s-wave phase shifts and an interference term between this and the resonance scattering. These expressions are given in reference (15); for the present purposes it will suffice to note that the angular dependence of the interference term is $P_\ell(\cos\theta)$.

The interpretation of the various terms in equation (29) may be given in order as: (1) pure Rutherford scattering, (2) interference between Rutherford and resonance scattering, (3) interference between Rutherford and potential or non-resonant scattering, (4) pure resonance scattering, (5) pure potential scattering, and (6) interference between resonance and potential scattering. In equation (30) the interpretation is similar except that there are no potential scattering terms.

Of particular interest in equation (30) is the angular dependence of the interference term which is $P_\ell(\cos\theta)$. Since the interference term with s-waves will also have this angular dependence, as mentioned above, an examination of resonances at the angles where $P_\ell(\cos\theta)$ vanishes is of particular significance; an interference effect at these angles ruling out the formation of the resonant state by the given ℓ-wave. It is true that interference with higher angular momenta may give such terms at these angles; however, the rapid increase of barrier penetration factor with ℓ make higher contributions unlikely, and in the present case they appear to a good approximation to be absent. It should be pointed out that the same consideration of barrier penetration

by higher ℓ-waves applies to the resonances and for this reason only the lowest possible ℓ value is considered in each case.

The absence of interference terms at the zeros of $P_\ell(\cos\theta)$ is, of course, also significant, but such results must be interpreted with care, especially at forward scattering angles, since the anomaly may be present but too small to be observed.

With these considerations we may now examine the scattering data for the qualitative conclusions which may be drawn from the angular distributions. The presence of appreciable interference terms at 90 and 125 degrees (the zeros of P_1 and P_2) imply that the 669, 843, 935, and 1422 kev resonances are s-wave; the angular momenta 1, 2, and 3 being excluded by the interference terms at these angles. Higher values are ruled out by the previous considerations and the fact that the interference term would vanish at some angle greater than 90 degrees causing a change of sign and an interchange of the relative positions of the maximum and minimum which does not appear to occur in any of these cases. Since the spin of F^{19} is $\frac{1}{2}$ with even parity,[16] the possible spin and parity values for these states are 0^+ and 1^+. The next step in the analysis is the comparison of the maximum variation of the cross section over the resonance, $\sigma_{max} - \sigma_{min}$, with the values calculated for each of the possible spin assignments. For this purpose values for the ratio Γ_p / Γ are needed. These may be obtained from the expression for the total reaction cross section,

$$\sigma_R = \frac{2J + 1}{(2i + 1)(2s + 1)} \frac{4\pi}{k^2} \frac{\Gamma_p \Gamma_R}{\Gamma^2} , \qquad (31)$$

and the condition $\Gamma = \Gamma_p + \Gamma_R$. In these expressions Γ_R is the reaction width, $\Gamma_\alpha + \Gamma_{p'}$ (neglecting the small reaction width). These expressions allow the determination of two values of Γ_p/Γ for each spin assignment thus giving four sets of parameters (Γ_p/Γ , J) for each of these resonances. The cross sections for (p,p') have recently been measured by Barnes,[2] and the cross sections used for (p,α) are the values determined by Barnes from the data of Chao, et. al.[17] and Freeman.[18]

For the 669 kev resonance values for the set (Γ_p/Γ, Γ_R/Γ) are (0.90;0.10) and (0.97;0.03) for J = 0^+ and 1^+ respectively. In either case the observed anomaly is much too large to allow the smaller value and is, in fact, in good agreement with the value calculated for J = 1^+ and Γ_p/Γ = 0.97. For J = 0^+ the anomaly would be smaller by the ratio of the statistical factors, 2J + 1, and this is clearly excluded. The observed and theoretical values are given in Table I.

At the 843 kev resonance the reaction cross sections are all small and therefore $\Gamma_p/\Gamma \cong 1$ for either J = 0^+ or 1^+. Here the size of the anomaly is in good agreement with 0^+ as shown in Table I.

For the 935 and 1422 kev resonances the reaction cross sections are too large to satisfy equation (31) for J = 0; in the former case the size indicates J = 1^+ and Γ_p/Γ = 0.175 and at 1422 kev Γ_p/Γ must be the larger value, 0.86, and again J = 1^+. These values are also given in Table I. It should be pointed out that the discrepancy between the observed and theoretical values for σ_{max} and σ_{min} at 935 kev is caused by the background from the 843 kev resonance; this effect is incoherent, however, since the

two resonances are formed by different channel spins.

For the remaining anomalies at 873, 1346, and 1372 kev, the absence of interference terms at 90 degrees and the increase in the size of the anomaly at larger angles suggest formation by p-waves, although the absence of data at 873 kev for forward angles and the fact that the 1346 kev resonance does not appear at forward angles make this conclusion tentative in these cases.

The 1372 kev resonance definitely shows anomalies at the forward scattering angles and seems, therefore, to be p-wave. For s-wave formation the observed reaction cross sections would exclude 0^+, and for 1^+ an anomaly of at least 30 percent of the Rutherford cross section would be expected at 90 degrees. For p-waves the assignment $J = 0^-$ is excluded by the reaction cross sections as above and by the presence of α emission to the 1^-, 2^+, and 3^- states in O^{16}, thus leaving the possible assignments 1^- and 2^-. In calculating the expected size of the anomaly in these cases the effects of interference with the 1422 kev resonance must be considered and, in addition, for 1^- we must allow the possibilities of both channel spins 0 and 1. The latter complication introduces an additional degree of freedom and this combined with the small size of the observed anomaly prevent a definite choice between 1^- and 2^-, as a reasonable fit may be obtained in either case. The presence of α-particles to the 1^-, 2^+, and 3^- states of O^{26} and the absence of transitions to the 0^+ states of this nucleus would seem to indicate, however, that the state is not 1^- in agreement with the results of Sanders[19] who found 2^-. The calculated values for this assignment are given

in Table I together with those observed in this experiment.

At the 1355 kev resonance the scattering results are not conclusive. The size of the anomaly would indicate that Γ_p/Γ was small, however, and the comparison of the observed and calculated values of $\sigma_{max}-\sigma_{min}$ given in Table I shows that the results are consistent with the assignment 2^- determined by Peterson, et. al.[3]

For the 873 kev resonance the assignment 2^- is well established from the (α,γ) correlation work of Seed and French.[20] As for the 1372 kev resonance, s-wave formation is excluded by the reaction cross sections for $J = 0^+$ and by the size of the anomaly at 90 degrees (about 20 percent of Rutherford) that would be expected for 1^+. P-wave formation would then imply 1^- and 2^- with 0^- excluded as at 1372. Again the possibility 1^- is not excluded by these data alone. The α-particle transition would again imply 2^-, however, and the agreement between the observed and theoretical parameters given in Table I shows that this is consistent. In this case difficulties are encountered due to the presence of the 843 kev level which gives interference effects; these would be less than about 20 percent however, and the reasonable agreement indicated that it was not worthwhile to calculate them.

In addition to the direct information obtained from the observed resonances, the absence of anomalies at other known resonances is, in general, an indication of a small proton width for the level. It is, of course, possible that certain angular dependences might cause the anomaly to be small at the particular

angles studied and that very narrow anomalies might be missed due to finite energy resolution. Where the spin, parity, and widths are known, however, it is usually possible to determine the size of Γ_p/Γ. For this reason an investigation of the regions near 340 and 480 kev at 160 degrees was made. The data from these experiments are quite poor due to target deterioration and no attempt to measure cross sections was made; it is believed that an anomaly of 10 to 20 percent of Rutherford could have been detected, however, whereas no anomaly was observed in either case. For the state at 340 kev the assignment is known[22] to be 1^+, and the reaction cross sections give either 1.0 or 0.016 for Γ_p/Γ. The larger value would predict an anomaly equal to the Rutherford cross section and rough estimates of the probable energy resolution indicate that this would not be diminished by more than a factor of three. Thus we conclude that Γ_p/Γ is small for this resonance.

For the 37 kev wide, 2^- state at 598 kev and the 19 kev wide, 3^+ state at 1290 kev the predicted values of Γ_p/Γ are again either near one or zero, and in both cases the absence of scattering anomalies would strongly indicate the smaller value.

The assignments determined from these experiments seem to be in reasonable agreement with the results of both the (p,p') and (p,α) experiments[2],[3],[17] with the exceptions of the 843 and 1422 kev states. For the 1422 kev level the (p,p') results are quite reasonable, showing a marked preference for decay to the 109 kev, $1/2^-$ state (by p-waves) over decay to the 196 kev, $5/2^+$ state (by d-waves). The absence of alpha particles to any of

the O^{16} states is, however, somewhat unusual considering the relatively strong short range alpha decays by the other 1^+ states. At the 843 kev level the weak transitions to either the F^{19} states (by p or d waves) or to the ground state of O^{16} (by s-waves) also seems anomalous. It is possible that this could imply an isotopic spin of 1 for these states, although the large number of states in F^{20} in this energy range would seem to indicate that there should be about as many T = 1 states as T = 0, and there seem to be only a few other levels which might appear to be T = 1.[2] The latter consideration suggests the hypothesis that all of the observed states are, in fact, T = 1, with the T = 0 states having very large widths for alpha decay. In this case the anomalous behavior of the 843 and 1422 levels would remain unexplained.

Table I

Resonance Parameters for $F^{19}(p,p)$

Proton Energy (kev)	Γ (kev) Γ_p/Γ	Ne^{20} J^π, ℓ_p		σ/σ_R					
				Observed			Calculated		
				max.	min.	diff.	max.	min.	diff.
669	7.5 0.98	$1^+,0$	90° 125° 160°	1.02 1.35 1.89	0.52 0.55 0.46	0.50 0.80 1.43	1.04 1.64 2.31	0.41 0.42 0.49	0.63 1.22 1.82
843	23 0.996	$0^+,0$	90° 125° 160°	1.07 1.27 1.55	0.86 0.88 0.89	0.21 0.39 0.66	1.03 1.20 1.54	0.80 0.72 0.82	0.23 0.48 0.72
873	5.2 0.21	$2^-,1$	90° 125° 160°	- ~1.22 ~1.43	- 1.14 1.06	- ~0.08 ~0.37	1.02 1.00 1.03	1.00 0.74 0.53	0.02 0.26 0.50
935	8.0 0.18	$1^+,0$	90° 125° 160°	1.09 1.24 1.39	0.99 1.02 1.11	0.10 0.22 0.28	1.02 1.10 1.19	0.85 0.83 0.85	0.17 0.27 0.34
1346	4.5 0.067	$2^-,1$	≤110° 125° 160°	- 1.09 1.12	- 1.07 1.07	- 0.02 0.05	 1.10 1.06	 1.01 0.87	≤0.034 0.09 0.19
1372	15 0.17	$2^-,1$	70° 90° 125° 160°	1.07 - 0.96 0.92	1.01 - 0.87 0.67	0.06 - 0.09 0.25	1.06 0.92 0.91	0.98 0.79 0.55	0.08 0.02 0.13 0.36
1422	14.6 0.86	$1^+,0$	53° 60° 70° 80° 90° 100° 110° 125° 136° 160°	1.08 1.03 1.00 1.11 1.27 1.41 1.61 1.98 2.17 2.74	0.74 0.69 0.61 0.66 0.58 0.60 0.68 0.64 0.63 0.63	0.34 0.34 0.39 0.45 0.69 0.81 0.93 1.34 1.54 2.11	1.01 1.00 1.01 1.08 1.23 1.42 1.69 2.15 2.49 3.06	0.64 0.56 0.48 0.41 0.37 0.36 0.36 0.39 0.42 0.44	0.37 0.44 0.53 0.67 0.86 1.06 1.33 1.76 2.07 2.62

A dash (-) indicates that no anomaly was observed. Resonance energies and widths are from reference (1) except for the energies 1346, 1372, and 1422 which are from reference (2). The observed values for 669 kev at 90 and 160 degrees are from evaporated LiF targets; the remainer are from pressed LiF targets. See Table III for values of $\sigma_{max} - \sigma_{min}$ corrected for energy resolution.

V. $N^{14}(p,p)$

1. Experimental Results

The results of these investigations are presented in Figures 13 and 14 as the ratio of the observed cross section to Rutherford cross section for proton energies from 1.0 to 1.1 and 1.4 to 1.8 Mev at scattering angles in the center-of-mass system of 90 and 125.3 degrees and in Figure 12 as the observed cross section for proton energies from 600 to 1800 kev at 154 degrees. For N^{14} + p the Rutherford cross section is:

$$\frac{d\sigma_R}{d\Omega_C} = \frac{0.07297}{E_1^2} \csc^4 \frac{\theta_C}{2} \quad \text{barns/steradian} \qquad (32)$$

The pronounced scattering anomalies occur near 1.06, 1.55, 1.75 and 1.81 Mev and are identified with the resonances in $N^{14}(p, \gamma)\, O^{15}$ reported by Duncan and Perry[5] at those energies. In addition to the sharp anomalies the cross section exhibits a marked variation from the Rutherford cross section over the entire range studied.

The determination of absolute cross sections for $N^{14}(p,p)$ was complicated by the erratic behavior of both the NH_3 and Be_3N_2 thick targets, and since the exact composition of the thin targets used was unknown, they could not be used for absolute determinations. In the case of both the NH_3 and Be_3N_2 targets individual determinations of the cross section varied over a range of about 20 percent, and the final normalization of the results was made by taking a weighted average of all determinations.

To obtain this average, each determination was assigned a weight involving the quality of the data and the estimated uncertainty in the solid angle calibration. The latter was appreciable for many of the values due to difficulties encountered in the determination of the solid angle at large scattering angles. This effect was presumably connected with the stray field of the magnetic spectrometer and manifested itself as a critical dependence of the effective solid angle on the incident beam position.

The majority of the determinations were made at 154 degrees at 1.0 Mev and the values of the cross section from NH_3 and Be_3N_2 at this point are 0.119 and 0.135 barns/steradian, respectively. The variance of the individual values from the mean is about 6 percent for NH_3 and 9 percent for Be_3N_2; however, the uncertainty in the stopping cross section for NH_3 is somewhat greater than for Be_3N_2 so that both values were given equal weight and the final value of the cross section at this point was taken as 0.127 barns/ster. with an estimated probable error of 10 percent.

The thick target profiles shown in Figure 2 indicate the uncertainties involved in both cases. For the ammonia targets the rapid deterioration is shown by the substantial decrease in yield with an old target as compared to a fresh target; this is seen to be accompanied by a large amount of carbon and oxygen contamination which presumably dilute the surface layers and cause the nitrogen yield to decrease.

For Be_3N_2 substantial amounts of oxygen were always found and did not seem to increase with bombardment, although carbon was accumulated. The correction to the calculated cross section due

to the presence of the oxygen, which was assumed to be distributed throughout the target material, is not as great as might appear from Figure 2 since in correcting for this both the yield from nitrogen and the effective stopping cross section per nitrogen atom must be altered, so that a change in the assumed nitrogen yield will cause only about a third this change in the calculated nitrogen cross section. The correction to the stopping cross section was made by taking the assumed oxygen background and from this yield calculating the amount of oxygen present, using the measured oxygen cross section[23] and assuming it to be in the form BeO. Determinations of the amount of oxygen were made at several energies for each of the targets used for excitation curves, and the average value for that target was used. The individual values ranged from about 3 to 10 percent BeO by weight and were reasonably consistent for any one target. An analysis of a sample of the Be_3N_2 by the Truesdail Laboratories, Inc. of Los Angeles, California gave 4.3 percent BeO, 90.5 percent Be_3N_2, 2.1 percent absorbed water, 2.5 percent free beryllium and traces of carbon.

To obtain the cross section at other angles and energies the relative values as determined by the thick and thin targets were used. For the thin target determinations the profiles in Figures 4 and 5 were compared by numerical integration using equation(25). These are divided into sets, representing determinations using the same target spot. Set 1 relates the cross section at 1.0 Mev at 125 and 154 degrees and 1.0 and 1.4 Mev at 90 degrees; set 2 relates 90, 125, and 154 degrees at 1.7 Mev; and set 3 relates 1.4 and 1.7 Mev

at 90 degrees.

At 1 Mev and 125 degrees the cross section relative to 154 degrees and 1.0 Mev was measured as 1.45 (1 1/4), 1.31 (1.0), and 1.26 (1 3/4) from Be_3N_2, NH_3, and the thin target, respectively. The numbers in brackets are the relative weights. This gives a weighted average of 1.33 with an estimated probable error of 6 percent. The thin target determinations only were available for the 1.4 to 1.7 Mev region at this angle and the two determinations at 1.4 and 1.7 Mev relative to 154 degrees are in good agreement with the relative value between 1.4 and 1.7 Mev as determined from the excitation curve. The profiles relating 1.4 Mev at 125 and 154 degrees are not shown since the 154 degree data were poor and the value from those data was given only a small weight in the final determination. The values relative to 1.0 Mev and 154 degrees are 0.81 at 1.4 Mev and 0.87 at 1.7 Mev with an estimated probable error of 6 percent.

At 90 degrees the values from the thin target determinations are again in good agreement and give 2.36, 1.37, and 1.26 at 1.0, 1.4, and 1.7 Mev, respectively, relative to 1.0 Mev at 154 degrees. The determination from the thick Be_3N_2 targets at 1.0 Mev and 90° is substantially higher than the thin target value, however, being 2.85 relative to 1.0 Mev and 154 degrees. NH_3 data at this angle were available but were quite poor and were therefore excluded; the values at 1.0 Mev ranged from 2.3 to 3.2. The thin target data (Figure 4) were difficult to interpret due to the large carbon and oxygen contamination and the same difficulty is present in the thick target determination (Figure 2). In addition, the thick target

values were obtained by using solid angle calibrations at large scattering angles and are also uncertain for that reason. The uncertainties in either case are about the same and the final value at 1.0 Mev and 90^{o} was taken as the average of the two, 2.65, with a probable error of 10-15 percent. This value was then used to adjust the thin target relative values to obtain the final cross sections at 90 degrees.

After obtaining the cross section at these points, the thin target results were converted to cross sections by assuming that these were proportional to the maximum yield (corrected for oxygen at 90 degrees as shown in Figure 4) and using the various reference points to determine the variation of the proportionality factor with energy. This is believed to be fairly reliable considering the short ranges over which the values must be extrapolated and interpolated and considering the slow variation in the proportionality factor which did not change by over a few percent per hundred kev in any case.

The slight difference in the energy scales of the thick and thin target experiments is probably due either to a change in the analyzer calibration or to the uncertainty in the spectrometer calibration for the thick target data. Precise energy determinations were not attempted; however, the electrostatic analyzer had been accurately calibrated on the 873.5 and 1372 kev resonances in $F^{19}(p,\alpha\gamma)$ shortly before this experiment and the energy scale is therefore probably accurate to a few kev, indicating that the resonance energies 1.064, 1.748, and 1.81 quoted by Duncan and Perry[5] are slightly high. In addition, the widths of the 1.55 and 1.75 Mev

resonances seem to be somewhat less than the values 50 and 11 kev, respectively, quoted by those authors.

2. Discussion

The analysis of $N^{14}(p,p)$ is simplified somewhat by the absence of other particle reactions, thus giving $\Gamma_p/\Gamma = 1.0$ in all cases. With this modification and the substitution of the appropriate statistical factors (i.e., $(2J + 1)/3$ for $(2J + 1)/2$) the s-wave contribution to the cross section for a given channel spin, 1/2 or 3/2, is then described by equation (29).

The angular variation of the 1.06 and 1.55 kev resonances strongly suggests formation by s-waves, and a preliminary analysis of the experimental results in terms of s-wave phase shifts indicates that both these resonances as well as the non-resonant cross section are well described in this manner. The spin and parity of N^{14} is 1^+ and therefore the corresponding states in O^{15} are either $1/2^+$ or $3/2^+$. The size of the 1.55 kev anomaly is in excellent agreement with the assignment $1/2^+$ given by Gove, et.al.[6] From equation (29) it may readily be shown that $\sigma_{max} - \sigma_{min}$ is independent of $\varphi_{1/2}$ and $\varphi_{3/2}$ (the non-resonant 1/2 and 3/2 s-wave phase shifts). The individual values of σ_{max}, σ_{min}, and the off resonance cross section do, however, depend strongly on these quantities and can be used to determine them. The calculated values given in Table II are for $\varphi_{1/2} = -0.25$ radians and $\varphi_{3/2} = -0.26$ radians. For the 1.06 kev resonance, the size is 15-25 percent larger than would be expected for $1/2^+$. For $3/2^+$,

however, the predicted size would be twice that for $1/2^+$, and an evaluation of the energy resolution effects by the techniques of Section VI would rule out this possibility if the resonance width, 4.8 kev, quoted by Duncan and Perry[5] is correct. In that case the discrepancy could be explained in part by an overestimate of the absolute cross section. If, however, the actual width is of the order of 3 kev, the correction to the size for the effects of finite energy resolution would be large enough to suggest $3/2^+$ for this state. Another determination of the width of this level would therefore be desirable. Calculated values for both assignments are given in Table II. The values of σ_{max} and σ_{min} for $J = 1/2^+$ are calculated for $\varphi_{1/2} = -0.05$ and $\varphi_{3/2} = -0.25$ radians.

For the two resonances at 1.75 and 1.81 Mev the angular variation suggests p-wave formation. In view of the large s-wave phase shifts implied by the variation of the cross section from Rutherford, the interference effects with the s-waves will strongly influence these anomalies and therefore need to be known with some accuracy. In particular, it is necessary to know the division of the s-wave phase shift into channel spins since only interference between like channel spins is possible. The assignment $J = 3/2^+$ at 1.06 Mev would give considerably different values for $\varphi_{1/2}$ and $\varphi_{3/2}$ than those quoted above for $J = 1/2^+$, and therefore the ambiguity in the assignment for this level complicates the extrapolation of the s-wave phase shifts to higher energies. For this reason an analysis of the 1.75 and 1.81 Mev levels has been made only at 90 degrees where the interference terms vanish.

At 90 degrees the size of both the 1.75 and 1.81 Mev anomalies

excludes the assignment $1/2^-$. The uncertainty in the absolute cross section and the width of the 1.73 Mev level as well as the relatively small size of the anomalies prevent a choice between $3/2^-$ and $5/2^-$, due to the uncertainty regarding the effects of resolution. The assignment $3/2^-$ for the 1.73 Mev level is suggested by Gove, et.al.[6]

The present results show no indication of either of the broad s-wave levels at 700 kev and 2.6 Mev reported by Duncan and Perry.[5] For the 2.6 Mev state this is not particularly significant since the highest energy observed in the present experiment is 1.8 Mev. It should be pointed out, however, that the broad rise in the cross section could not be caused by this level since s-wave resonances at this angle will cause the cross section to be lower below the resonance than above. For the reported width[5] (1.3 Mev) of this level this effect should be observed in the present energy range, although it is not unreasonable that it could be masked by other s-wave phase shifts.

The presence of the 700 kev level would seem, however, to be excluded by the present experimental results. For the case giving the smallest anomaly, $J = 1/2^+$, calculated values of the ratio of the maximum and minimum cross sections to the Rutherford cross section are given in Table II. The maximum would occur between 700 and 800 kev and the cross section would drop to about 1.1 times Rutherford at 1.0 Mev. Such a large variation in the cross section seems clearly incompatible with the present results. For higher orbital angular momenta the anomaly would be as large or larger unless particular angular variations caused it to be small at this angle. This would seem unlikely for reasonable values of ℓ, however.

A further investigation of the scattering at lower energies and other angles would be of considerable value.

Table II

Resonance Parameters for $N^{14}(p,p)$

Proton Energy (Mev)	Γ (kev) ($\Gamma_p = \Gamma$)	O^{15*} J^{π}, ℓ_p	θ_c	σ/σ_R					
				Observed			Calculated		
				max.	min.	diff.	max.	min.	diff.
1.06	4.8	$1/2^+,0$	90°	1.51	0.87	0.64	1.54	0.96	0.58
			125°	2.48	1.15	1.33	2.32	1.27	1.05
			154°	2.96	1.30	1.66	2.92	1.45	1.47
		$3/2^+,0$	90°			0.64			1.06
			125°			1.33			2.10
			154°			1.66			2.94
1.55	36	$1/2^+,0$	90°	1.60	1.01	0.59	1.60	1.00	0.60
			125°	2.60	1.30	1.30	2.70	1.39	1.31
			154°	3.57	1.58	1.99	3.56	1.58	1.98
1.73	~5	$1/2^-,1$	90°			0.63			0.47
		$3/2^-,1$	90°			0.63			.47-.94
		$5/2^-,1$	90°			0.63			1.02
1.79	7	$1/2^-,1$	90°			0.58			0.49
		$3/2^-,1$	90°			0.58			.49-.98
		$5/2^-,1$	90°			0.58			1.06
0.7	100	$1/2^+,0$	154°	Not observed			1.87	0.74	1.13

The widths of the 1.06 and 1.79 Mev resonances are from reference (5). See Table III for values of $\sigma_{max} - \sigma_{min}$ corrected for energy resolution.

V. ENERGY RESOLUTION

1. General

In the determination of cross sections for nuclear reactions we are interested in measuring the number of reactions per incident particle when the incident particles have a given energy immediately before the reaction. In principle, we bombard a target with a homogeneous beam and observe the number of particles leaving the target in a given direction in a given energy range determined by the target thickness or the resolution of our detector, whichever is smaller. This finite energy range of observations immediately presents a source of inherent energy spread, however, since the yield will vanish if we decrease the target thickness or the resolution indefinitely. At the same time this source of energy spread introduces another; straggling in the energy loss in the target. This is especially important in thick target work where the lamina of observation may be located at a depth several times its own thickness. The finite solid angle of observation may also be regarded as an inherent source of energy spread since again the yield of the reaction is proportional to the solid angle.

In addition to these sources there will always be other effects which are not inherent in the technique but which represent practical limitations. These include the finite incident beam size resulting in an extended source at the target, inhomogenity of the incident beam energy and target surface irregularities.

The result of these effects is a smearing of sharp resonance

structures in the cross section curve which will, of course, become more pronounced as the width of the structure becomes smaller. In an attempt to evaluate these effects in thick target scattering experiments, Cohen[24] has calculated the approximate energy spread due to the following effects: (1) finite beam size, (2) energy variation in the incident beam, (3) finite spectrometer solid angle, (4) finite spectrometer exit slit (finite resolution of the spectrometer), and (5) straggling in the energy loss in the target. As applied to the present experiments, the overall root-mean-square energy variation due to these effects is about 2 kev at 1 Mev proton bombarding energy. This increases roughly linearly with energy. Cohen's procedure was to use the total root-mean-square variation calculated on this basis to obtain the approximate corrections to the maximum and minimum cross sections of the scattering anomalies in cases where the energy variation was small compared to the resonance width.

Corrections of this type as applied to the present experimental results, however, give values which are appreciably smaller than the theoretical calculations for the variations of the cross section, and additional experimental and theoretical investigations indicate that the actual energy variation is appreciably larger than Cohen's values. It is believed that an important contribution to this is the irregularity of the target surface. Calculations of the size of this effect are rather difficult, although one can easily estimate an upper limit by considering the energy relations in the target discussed in Section III. In the usual target arrangement the angles θ_1 and θ_2 are made equal, so that the normal to the target

bisects the angle between the incident beam direction and the direction of observation. In this case approximately half the energy loss in the target occurs before scattering. If, however, the target surface were sufficiently irregular, then it would be possible for the entire energy loss to occur either before or after scattering. An estimate of the upper limit of this effect would thus be a square distribution of total width twice the "following energy". This would be about 2% of the bombarding energy, or about 20 kev at 1 Mev, and would give a root-mean-square variation of the order of 5-6 kev. Since the energy thickness of any surface irregularity would decrease with energy and since the depth of the lamina of observation would increase, we would expect this effect to be most pronounced at the lower energies, and since the extreme cases occur only when the target surface is approximately parallel or perpendicular to the incident beam direction, we would also expect the effect to be most pronounced for small scattering angles where these conditions are most likely to obtain.

Microscopic examination of the lithium fluoride powder used in preparing targets for the $F^{19}(p,p)$ investigations indicates that the grain size is about 10^{-4} cm, which is of the order of five times the depths at which scattering occurs in the target. This suggests that the surface irregularities (assumed to be determined by individual grains) are of this same order and therefore may affect substantially the energy resolution.

Some experimental investigations have been made which also indicate this effect. In Cohen's formulation the energy straggling

is the only quantity which depends on the depth of scattering in the target, and this effect can be calculated to a reasonable accuracy. The target irregularity effect should also depend on the "following energy" so that a direct measurement of the resolution as a function of the depth of scattering is of considerable interest. Such a measurement was made by observing the yield at the minimum of the 1422 kev resonance in $F^{19}(p,p)$ at 90 degrees as a function of the scattering depth in the target. By extrapolating these measurements to zero energy loss before scattering, and using the relations between the observed cross section and resolution derived below, a value of δE_F, the root-mean-square energy variation due to energy loss in the target, can be obtained. In a typical experiment, we find for a "following depth" of 15 kev, $\delta E_F \cong 3.3$ kev, while the value for straggling alone is 2.0 kev. A square window of 30 kev (twice the "following energy") would give about 8-9 kev, so that a contribution of only one third this would be needed to explain the observed value.

Another indication that the target surface condition may substantially affect the energy resolution is provided by a comparison of the 669 kev resonance in $F^{19}(p,p)$ as observed with pressed and evaporated LiF targets under the same conditions. These results are shown in Figure 7. A comparison of the pressed Be_3N_2 targets and the thin target used for the $N^{14}(p,p)$ investigations is given in Figures 13 and 14 for the 1.06, 1.55, and 1.73 Mev resonances.

Since the size of the surface effect is difficult to estimate very accurately in any given case and since there could also be other unknown effects contributing to the energy variation, it

seemed desirable to develope a procedure for estimating the overall energy resolution directly. Such a procedure can easily be found in the case of gamma ray or reaction resonances since the total area under the resonance curve will be constant regardless of the target thickness or other energy resolution. Thus, for a square resolution function, the observed width, Γ_o, the actual resonance width, Γ, and the window (or target) width, α, are related as,

$$\Gamma_o^2 = \Gamma^2 + \alpha^2 \quad ,$$

and the maximum yield will vary in such a way that the area under the curve is constant. In the case of an elastic scattering resonance the total area is, in general, infinite, and this procedure does not apply directly. We can, however, approach the problem in a similar manner by using the increase in some characteristic width of the structure to evaluate the total resolution and, hence, to obtain the size of the anomaly.

The maximum variation of the cross section over the resonance, $\sigma_{max} - \sigma_{min}$, has been shown to be a quantity of considerable interest in determining spin assignments from observations of elastic scattering. Our procedure is to obtain the corrected value of this quantity directly in terms of observable parameters of the resonance curve.

We consider the theoretical expressions (29) and (30) for the cross section in the vicinity of a resonance. Substituting $x = \frac{E - E_R}{\Gamma/2}$, these may be shown to take the general form,

$$\sigma = \sigma_o \left[1 + f(x)\right] \qquad (33)$$

$$f(x) = \frac{a + bx}{1 + x^2}$$

where a, b, and σ_o are approximately independent of energy and are considered to be unknown. σ is the ratio of the cross section to the Rutherford cross section.

The energy resolution function, P(E,E'), is defined as the probability that the reaction energy is E' when the average reaction energy is E, or in terms of x, we have P(x,x'). The observed cross section, $\bar{\sigma}$, will then be:

$$\bar{\sigma}(x) = \int_{-\infty}^{+\infty} \sigma(x')\, P(x,x')\, dx' \qquad (34)$$

or,

$$\bar{\sigma} = \sigma_o \quad (1 + F(x)), \text{ where}$$

$$F(x) = \int_{-\infty}^{+\infty} f(x)\, P(x,x')\, dx' \quad . \qquad (35)$$

We define $K = \dfrac{\bar{\sigma}_{max} - \bar{\sigma}_{min}}{\sigma_{max} - \sigma_{min}}$, and we wish to determine K in terms of other parameters of the resonance as outlined above. For this purpose we assume a particular form for the distribution function:

$$P(x,x) = \frac{1}{2\alpha} \quad \text{for} \quad |x-x'| \leq \alpha$$

$$P(x,x) = 0 \quad \text{for} \quad |x-x'| \geq \alpha$$

Then,

$$F(x) = \frac{1}{2\alpha}\left[a \tan^{-1} \frac{2\alpha}{1 + x^2 - \alpha^2} + \frac{b}{2} \log \frac{1 + (x + \alpha)^2}{1 + (x - \alpha)^2}\right] \qquad (36)$$

$$\frac{dF}{dx} = 0 \text{ at } x_{1,2} = \frac{-a \pm \left[a^2 + b^2 (1 + \alpha^2)\right]^{1/2}}{b} \qquad (37)$$

$$y \equiv \frac{E_{max} - E_{min}}{\Gamma} = (1 + \alpha^2 + a^2/b^2)^{1/2} \qquad (38)$$

$$A \equiv \left[\frac{F(x_1)}{F(x_2)}\right] = \frac{\tanh^{-1}\frac{\alpha}{y} - \frac{a}{b}\tan^{-1}\frac{2\alpha}{1 + x_1^2 - \alpha^2}}{\tanh^{-1}\frac{\alpha}{y} + \frac{a}{b}\tan^{-1}\frac{2\alpha}{1 + x_2^2 - \alpha^2}} \qquad (39)$$

$$K = \frac{1}{\alpha}\frac{1}{(a^2 + b^2)^{1/2}}\left[a\tan^{-1}\frac{\alpha a}{yb} + b\tanh^{-1}\frac{\alpha}{y}\right] \qquad (40)$$

where E_{max} and E_{min} are the proton energies for which the maximum and minimum values of the cross section are observed. A and y are defined by these equations and the condition that $A \leq 1$.

The effects of energy variation are thus seen to be an increase in $E_{max} - E_{min}$ and a decrease in K. Our procedure involves the evaluation of the latter effect by observing the former. The additional parameter A is introduced since we have treated both α and a/b as parameters to be determined. In principle, a, b, and σ_o may be calculated if the assignments for the level and the non-resonant phase shifts are known; however, these results are somewhat sensitive to the choice of the latter quantities while the value of K is relatively insensitive to A and hence to σ_o. We have found that a visual estimate of σ_o (to about 10%) is usually satisfactory. This procedure also permits the correction of the data independent of the level assignment.

To obtain the explicit relation between K, A, and y, we first use equation (39) to obtain, graphically, A as a function of a/b, treating α as a parameter. This is shown in Figure 15. Using this relation and equations (38), (39), and (40), we may then obtain y, A, and K for any a/b and α, and in this way construct a graphical relation between y, A, and K. This is given in Figure 16, where

K is given as a function of y, with A treated as a parameter. To apply this to a given resonance, we observe σ_{max}, σ_{min}, E_{max}, and E_{min} and estimate σ_o. (σ_o is the non-resonant cross section; see equation (33)) We then calculate A and y using the definitions (38) and (39), and from Figure 16 obtain K.

In many cases E_{max} or E_{min} is not well defined, and it is possible to use the width at half maximum (or minimum) instead of y in these cases. This width cannot be obtained explicitly in terms of α and a/b, however, so an additional graphical or numerical solution is necessary in this case. Using Figure 15 we find values of α and a/b for a given A, and for each set (a/b, α) we solve numerically for $z = \frac{\text{width at half maximum}}{\Gamma}$, and use equation (40) to obtain K. In this way we find K as a function of z, for various values of A as shown in Figure 17. This relation is, however, usually much harder to apply than the former since it requires more accurate estimates of σ_o, and it is generally of value only in cases where the scattering anomaly is nearly symmetric. For the latter case this procedure reduces to the treatment outlined above for gamma ray or reaction resonances.

An interesting relation may be obtained by taking the product x_1x_2; from equation (37):

$$-x_1x_2 = \frac{(E_{max} - E_R)(E_R - E_{min})}{(\Gamma/2)^2} = 1 + \alpha^2 \qquad (41)$$

In principle, this relation would allow the explicit determination of K in terms of E_{max}, E_{min}, and E_R by using equations (38), (40), and (41). In practice, however, this requires that the resonance

energy be known relative to the maximum and minimum (i. e., be known on the energy scale of the experiment) with an uncertainty small compared to the half-width. In general, this condition is not well satisfied. In the present experiments, for example, the uncertainty in the absolute energy scale is about 3 kev, while many of the resonances have total widths of the order of 5 to 10 kev.

By obtaining the final expressions as relations between experimentally determined quantities it might be hoped that the dependence of the results on the particular form assumed for the distribution function would not be too great. To investigate this we may compare the above results with those obtained by assuming the function:

$$P(x,x') = \frac{\beta}{\pi} \frac{1}{\beta^2 + (x - x')^2} \tag{42}$$

This gives for F(x):

$$F(x) = \frac{a + b\,\bar{x}}{(1 + \bar{x}^2)}, \qquad \text{where } \bar{x} = \frac{x}{1 + \beta} \tag{43}$$

In this case the explicit expressions for K as a function of y, z and A may be obtained. They are:

$$K = \frac{A + 1}{2A^{1/2}\,y} \tag{44}$$

$$K = \frac{(2A + 1)^{1/2}}{z} \tag{45}$$

For comparison with the earlier results values of K calculated from these expressions are included in Figures (16) and (17). It will be noted that, in general, the values for K from equation (44) and (45) are appreciably lower than those from the square distribution. It would seem, however, that the latter is the more realistic approximation considering the extreme tail on the distribution (42) which is almost certainly not realized in practice. On the other hand, the comparison does indicate that the corrections calculated for the square distribution might be small.

The assumed form for the resonant cross section, (33), should be a close approximation in most cases where resolution is important since the variation of the parameters a, b, and σ_o will be quite small over narrow resonances. The case of two rapidly varying phase shifts, as would be encountered for two resonances with a separation comparable to their widths, would require special treatment.

2. Applications to $F^{19}(p,p)$ and $N^{14}(p,p)$

Corrected values for $\sigma_{max} - \sigma_{min}$ (using the square distribution function) for several of the resonances observed in these experiments are given in Table III together with the observed and theoretical values from Tables I and II. Observed and calculated values of the full window width ($\propto \Gamma$) are also given as well as the parameters A and y or z. The corrections are made in all cases using the widths given in Tables I and II.

Table III

	E_R (kev)	θ_c	$\frac{\sigma_{max}-\sigma_{min}}{\sigma_R}$			A	y	z	Window Width ($\propto\Gamma$) (kev)		
			Obs.	Corr.	Theory				Obs.	Calculated	
										Cohen	Surf. (a)
$F^{19}(p,p)$ pressed LiF target	669	90°	0.37	0.61	0.63	0.1		2.13	14	4.8	16
		125°	0.80	1.01	1.22	1.0	1.84		12	4.1	12
		160°	1.21	1.51	1.82	0.5	1.77		11	3.6	10
	935	90°	0.10	0.20	0.17	0.5		2.45	18	6.5	18
		125°	0.22	0.31	0.27	0.4	2.19		15	6.0	16
		160°	0.28	0.33	0.34	1.0	1.59		9	5.2	12
	1422	70°	0.39	0.52	0.53	0		1.50	16	8.5	30
		100°	0.81	0.88	1.06	0.4	1.40		11	8.4	28
		125°	1.34	1.47	1.76	0.8	1.31		12	8.0	24
		160°	2.11	2.18	2.62	0.6	1.12		6	7.4	18
$F^{19}(p,p)$ evaporated LiF target	669	90°	0.50	0.57	0.63	0.1		1.40	7	4.8	16
		160°	1.43	1.49	1.82	0.5	1.18		4	3.6	10
$N^{14}(p,p)$ Thick Be_3N_2 target	1060	154°	1.18	1.85	(b)	0.4	2.50		11	~5	12
	1730	154°	1.95	4.54		0.1		3.25	16	~10	35
$N^{14}(p,p)$ Thin target	1060	125°	1.33	1.46	(b)	0.5	1.33		3.8		
		154°	1.66	1.69	(b)	0.3	1.31		2.4		
	1730	90°	0.63	1.05	(b)	0	~2.0		~9		
		154°	6.15	6.15		0.1	~1.0				
	1790	90°	0.58	0.89	(b)	0	~1.8		~10		

(a) Estimated upper limit for surface irregularity

(b) See Table II

In considering the effects of energy distribution on observed cross sections, we have thus far only considered the effects on rapidly varying parts of the cross section curve, and it is of interest to consider whether or not these conditions can affect the yield in the slowly varying regions. For this purpose we consider again the expression (17), which gives the yield in terms of the observables in the experiment:

$$Y \sim \frac{\sigma \Omega q E_{20}}{R_c \epsilon_{eff}} \qquad (46)$$

Since the non-resonant elastic scattering is primarily Rutherford, the maximum variation of the cross section over the energy and angular ranges involved is quite small and the change in the yield averaged over these variations is negligible in most cases. For the present purposes we may neglect this variation and assume the cross section off resonance to be constant. The variation in E_{20} due to the finite resolution of the spectrometer has already been taken into account in obtaining equation (17), so the only remaining quantity in this equation which could give rise to appreciable variations is ϵ_{eff}. From equation (14),

$$\epsilon_{eff} = (k + \eta)\epsilon_1 = \left[\frac{\partial E_2}{\partial E_1} + \frac{\epsilon_2 \cos \theta_1}{\epsilon_1 \cos \theta_2}\right]\epsilon_1 \qquad (47)$$

In the normal target arrangement, $\theta_1 = \theta_2$; however, in consideration of the possibility of surface irregularities, we need to consider the effect of this on ϵ_{eff} and hence on the observed yield. We put $\theta_1 = \theta_o + \varphi$, $\theta_2 = \theta_o - \varphi$, and define

$$p(\varphi) = \frac{Y(\varphi)}{Y(o)} = \frac{k\epsilon_1 + \epsilon_2}{k\epsilon_1 + \epsilon_2 \frac{\cos\theta_1}{\cos\theta_2}} = \frac{k + \eta_o}{k + \eta} \qquad (48)$$

To estimate the approximate size of this effect, we make the assumption previously used; that all angles φ are equally probable (i. e. that any energy loss before scattering is equally probable), and we ask for the observed yield,

$$\bar{p} = \frac{1}{2\theta_o} \int_{-\theta_o}^{+\theta_o} p(\varphi)\, d\varphi \qquad (49)$$

Clearly the symmetric part of p will give zero in (49), so we resolve p into its symmetric and antisymmetric components and consider only the latter, $g(\varphi)$, thus:

$$\bar{p} = \frac{1}{\theta_o} \int_{o}^{\theta_o} g(\varphi)\, d\varphi \qquad (50)$$

we put $k = 1 - \epsilon_1$, $\eta = 1 + \epsilon_2$, and expand $g(\varphi)$ for $\epsilon_1, \epsilon_2 \ll 1$. Thus,

$$g(\varphi) \cong 1 + \frac{\epsilon_1 + \epsilon_2}{2} \tan^2\theta_o \tan^2\varphi = 1 + \frac{\eta_o - k}{2} \tan^2\theta_o \tan^2\varphi$$

and,

$$\bar{p} \cong 1 + \frac{\eta_o - k}{2} \tan^2\theta_o \left[\frac{\tan\theta_o}{\theta_o} - 1\right] \qquad (51)$$

where the scattering angle, $\theta = \pi - 2\theta_o$. For the present purposes it is sufficiently accurate to assume that the stopping cross section varies as the inverse square root of the energy, thus,

$$\bar{p} \cong 1 + \frac{3}{4}(1 - k) \tan^2\theta_o \left[\frac{\tan\theta_o}{\theta_o} - 1\right] \qquad (52)$$

At a scattering angle of 90 degrees this amounts to less than a 3 percent increase in yield for either F^{19} or N^{14} ; at 60 degrees, however, it gives about 7 percent for fluorine and 10 percent for nitrogen and could therefore represent an appreciable error at forward scattering angles.

APPENDIX

Stopping Cross Sections

1. LiF

The relative stopping cross section was obtained by evaporating a thin layer of LiF on a copper backing and observing the protons elastically scattered from the copper after traversing the LiF layer.[11] These values were normalized to 8.42×10^{-15} ev-cm^2 at 1 Mev by assuming the stopping cross section for LiF to be the sum of the stopping cross sections for lithium and fluorine at this energy. The lithium value was obtained from the absolute measurement by Bader[25] which was used to normalize the relative values measured by Warters.[11] The fluorine value was obtained from the measured proton stopping cross section for neon,[21],[26] using 4 Mev alpha-particle data for neon[13],[14] and oxygen[14],[27] to determine the value for fluorine relative to neon. This procedure was believed to be more reliable at high energies, and for this reason the normalization was made at 1 Mev, the highest energy for which proton data for neon was available. Oxygen[21] and neon[21],[26] proton data are both available at 600 kev, and normalization at this point gives values about 3 percent lower than those used. The final values for LiF are presented in Figure 17, together with the values for lithium from Bader[25] and Warters[11] and the values for fluorine taken as the difference of these.

A direct measurement of the stopping cross section for protons in LiF has recently been made by Bader[25] for proton energies below 600 kev, and the values given in Figure 17 agree with those determined by Bader within 3 percent.

2. NH_3

Absolute stopping cross sections for protons in ammonia gas have been measured for proton energies below 550 kev;[21] these values were assumed to hold for solid ammonia and were used to determine the effective ionization potential in the Bethe stopping cross section formula with K-shell correction. These results give I = 68 ev and,

$$\epsilon = \frac{239}{E}\left[10 \ln \frac{E}{31.4} - C_K\right] \qquad (53)$$

with E in kev. Since measured stopping cross sections were not available for hydrogen, there was no way to cross check these values, and they could probably be in error by several percent at the higher energies.

3. Be_3N_2

Absolute stopping cross sections for protons in nitrogen gas have been determined by Chilton, et.al.[26] for energies below 1.0 Mev and by Reynolds, et.al.[21] for energies below 550 kev. These values are in good agreement and give an ionization potential of 90 ev. Using this value for I in the Bethe expression,

$$\epsilon_N = \frac{239}{E} \left[7 \ln \frac{E}{41.7} - C_K \right] \qquad (54)$$

For protons in beryllium, Bader's[25] absolute determination was used to normalize the relative values measured by Mozer.[28] These values turn out to be (within 2 percent) 2/3 of the values calculated for nitrogen from (54) over the entire energy range 600 to 1800 kev. Thus, assuming the stopping cross section per nitrogen atom to be the sum of three halves the Be value and the nitrogen value, we have, with E in kev,

$$\epsilon = \frac{478}{E} \left[7 \ln \frac{E}{41.7} - C_K \right] \qquad (55)$$

In this case the error in extrapolation of the nitrogen results is probably small since the calculated values are in good agreement with the experimental results below 1.0 Mev, and the theoretical expression should be more reliable at higher energies.

REFERENCES

1. F. Ajzenberg and T. Lauritsen, Revs. Mod. Phys. 27, 77 (1955)
2. C. A. Barnes, Phys. Rev. 97, 1226 (1955)
3. Peterson, Fowler, and Lauritsen, Phys. Rev. 96, 1250 (1954)
4. G. Dearnaley, Phil. Mag. 45, 213 (1954)
5. D. B. Duncan and J. E. Perry, Phys. Rev. 82, 809 (1951)
6. Gove, Ferguson, and Sample, Phys. Rev. 93, 928A (1954)
7. Tautfest, Havill, and Rubin, Bull. Amer. Phys. Soc. 29, 32 (1954) and private communication
8. Lauritsen, Lauritsen, and Fowler, Phys. Rev. 59, 241 (1941)
9. E. A. Milne, Ph. D. Thesis, California Institute of Technology (1953)
10. Fowler, Lauritsen, and Lauritsen, Phys. Rev. 18, 818 (1947)
11. W. D. Warters, Ph. D. Thesis, California Institute of Technology (1953)
12. Brown, Snyder, Fowler, and Lauritsen, Phys. Rev. 82, 159 (1951)
13. G. Mano, Ann. der Physique 1, 408 (1934)
14. R. W. Gurney, Proc. Roy. Soc. A107, 340 (1925)
15. E. Baranger, Phys. Rev. (to be published)
16. A. P. French and J. O. Newton, Phys. Rev. 85, 1041 (1952)
17. Chao, Tollestrup, Fowler, and Lauritsen, Phys. Rev. 79, 108 (1950)
18. J. M. Freeman, Phil. Mag. 41, 1225 (1950)
19. J. E. Sanders, Phil. Mag. 44, 1302 (1953)
20. J. Seed and A. P. French, Phys. Rev. 88, 1007 (1952)
21. Reynolds, Dunbar, Wenzel, and Whaling, Phys. Rev. 92, 742 (1953)
22. Barnes, French, and Devons, Nature 166, 145 (1950)

23. F. Eppling, Ph. D. Thesis, University of Wisconsin (1952)

24. E. R. Cohen, Ph. D. Thesis, California Institute of Technology (1949)

25. M. Bader, Ph. D. Thesis, California Institute of Technology (1955)

26. Chilton, Cooper, and Harris, Phys. Rev. 93, 413 (1953)

27. G. E. Gibson and H. Eyring, Phys. Rev. 30, 553 (1927)

28. F. S. Mozer, private communication

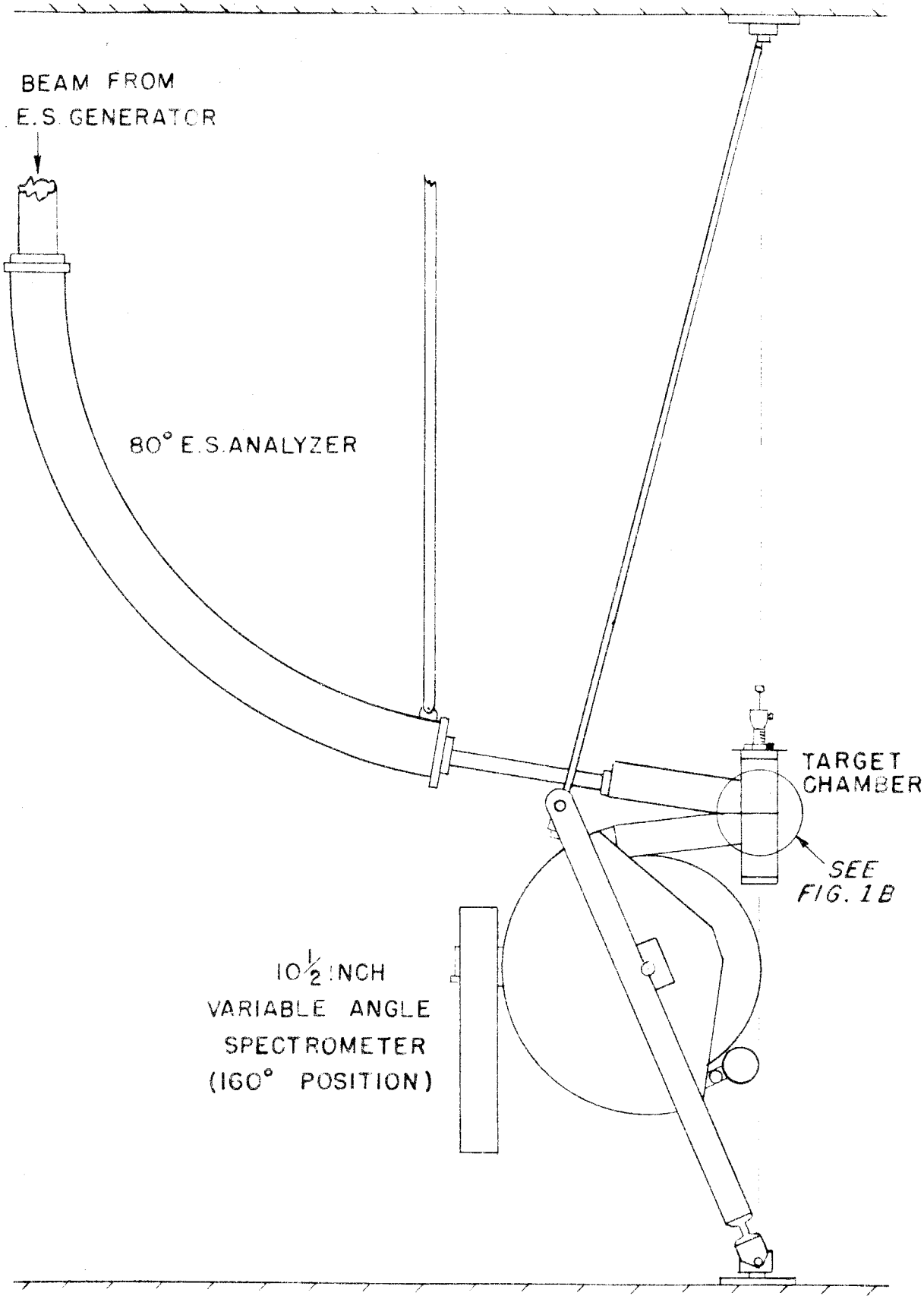

FIGURE 1A - LAYOUT OF APPARATUS

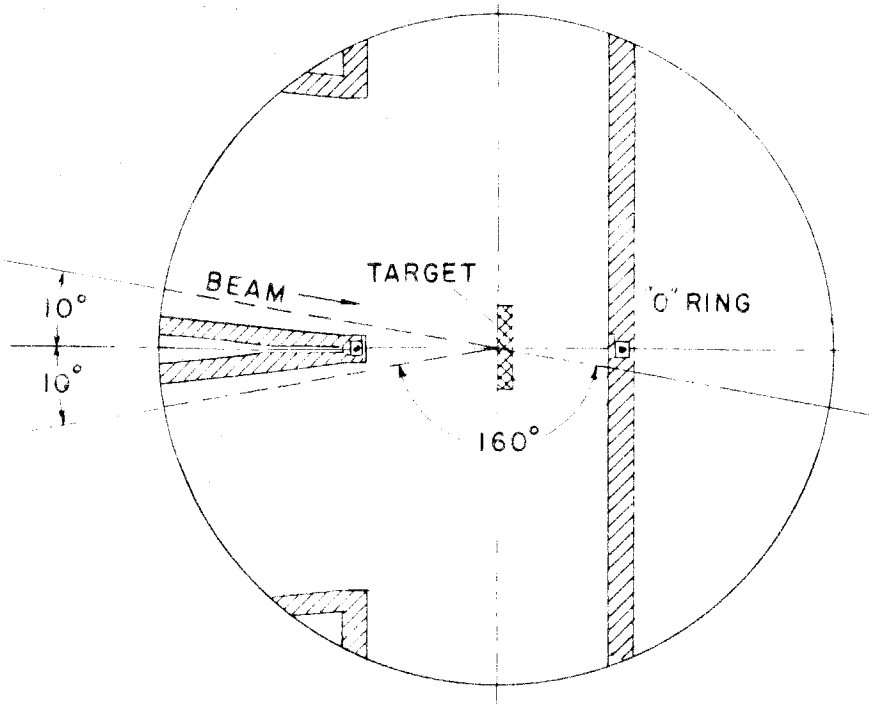

160° POSITION

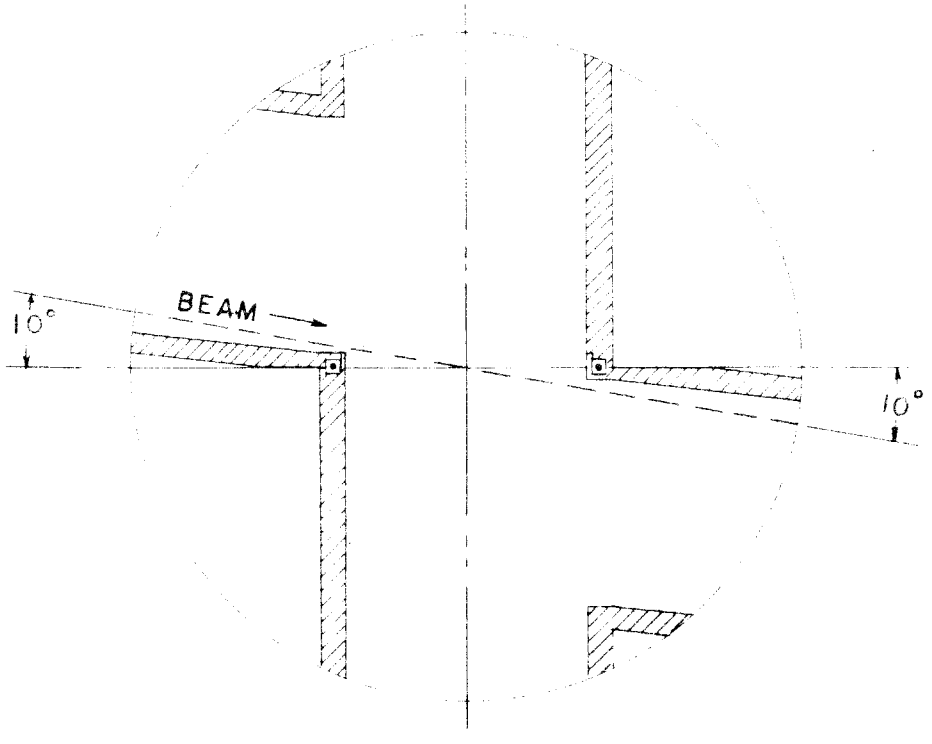

0° POSITION

FIGURE 1B – TARGET CHAMBER DETAIL

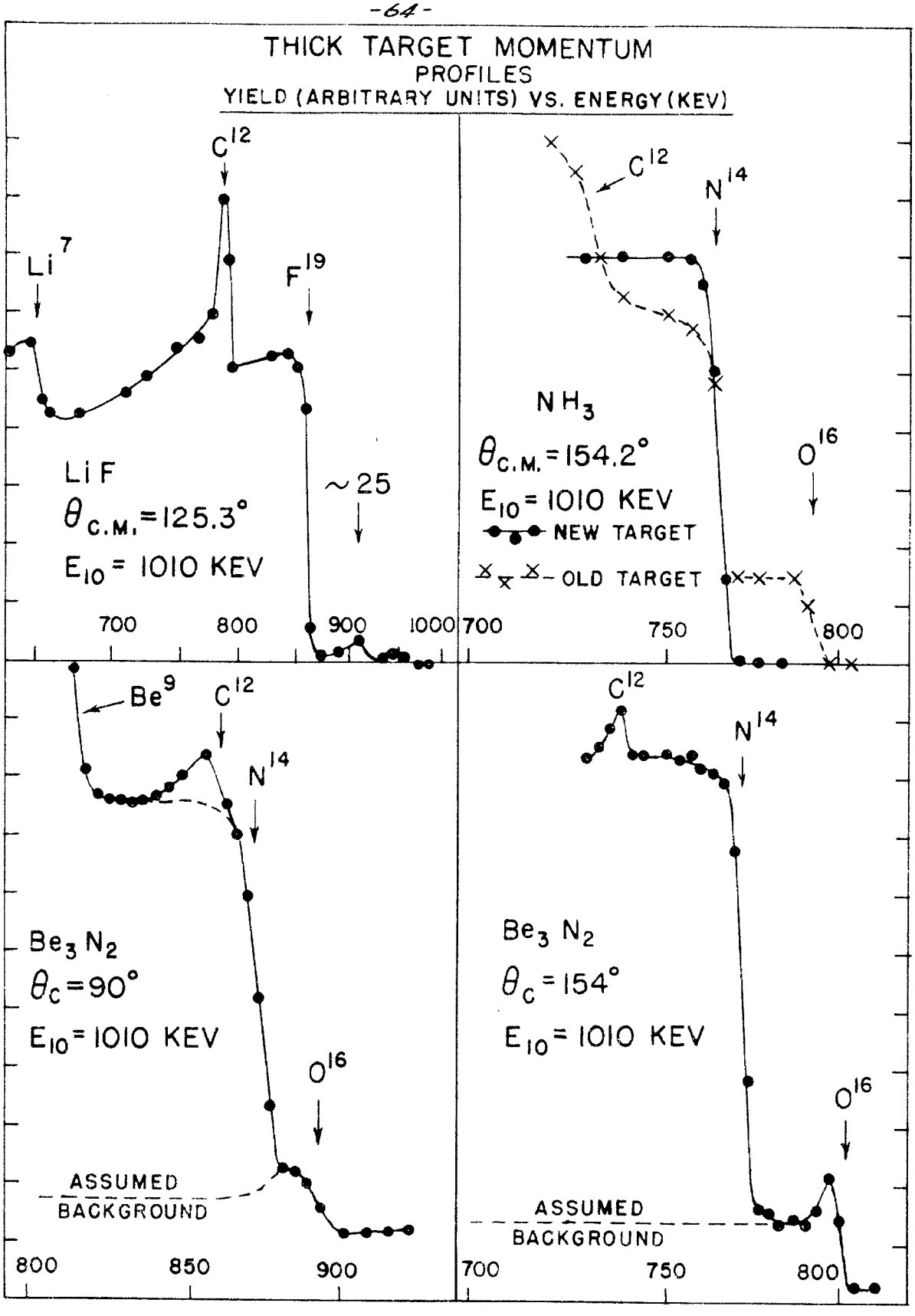
THICK TARGET MOMENTUM
PROFILES
YIELD (ARBITRARY UNITS) VS. ENERGY (KEV)
Li7
C12
F19
~25
LiF
θc.m.=125.3°
E10 = 1010 KEV
700
800
900
1000
C12
N14
NH3
θc.m.=154.2°
E10 = 1010 KEV
NEW TARGET
OLD TARGET
O16
700
750
800
Be9
C12
N14
Be3N2
θc=90°
E10 = 1010 KEV
O16
ASSUMED BACKGROUND
800
850
900
C12
N14
Be3N2
θc=154°
E10 = 1010 KEV
O16
ASSUMED BACKGROUND
700
750
800

FIGURE 2

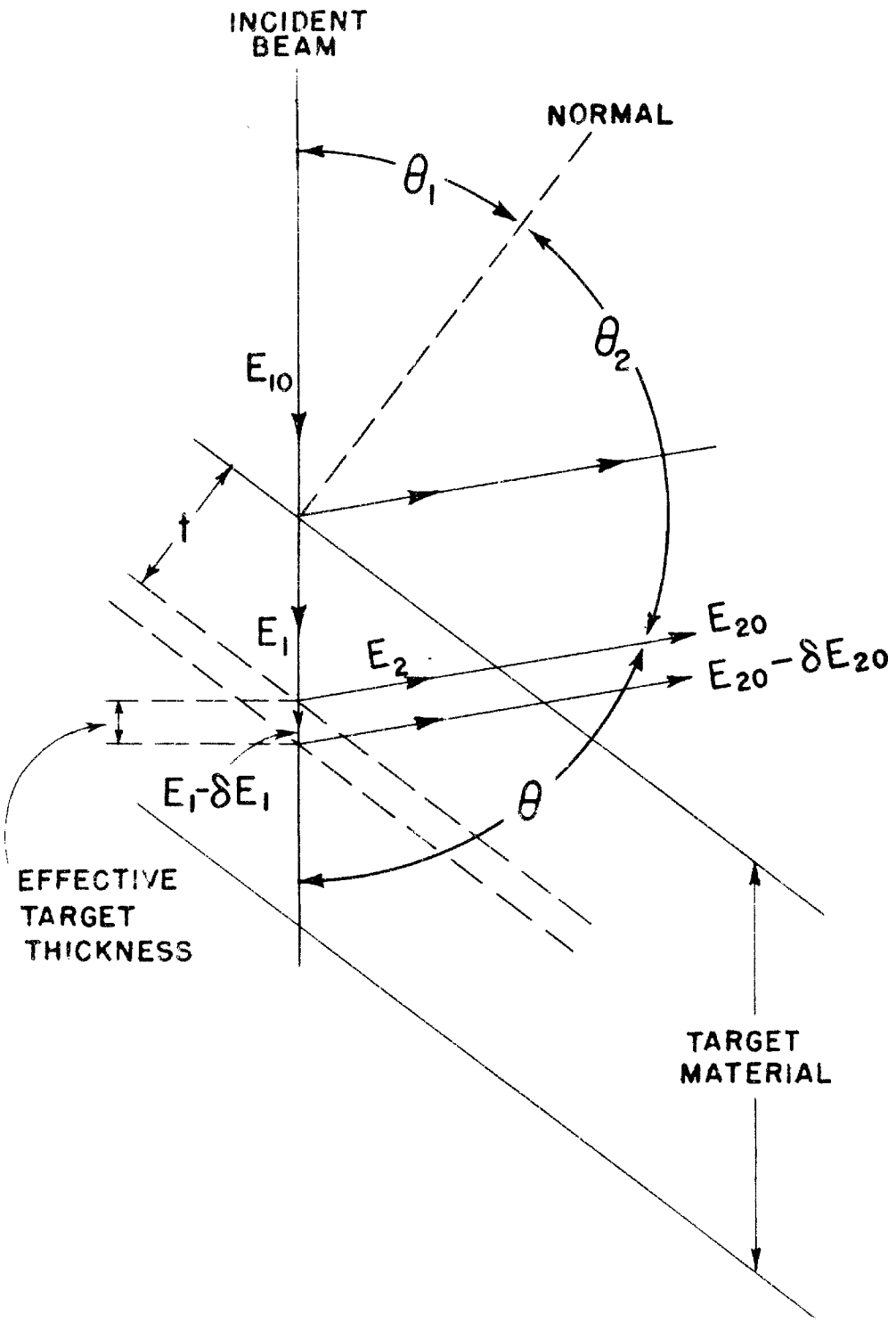

FIGURE 3
THICK TARGET ENERGY RELATIONS

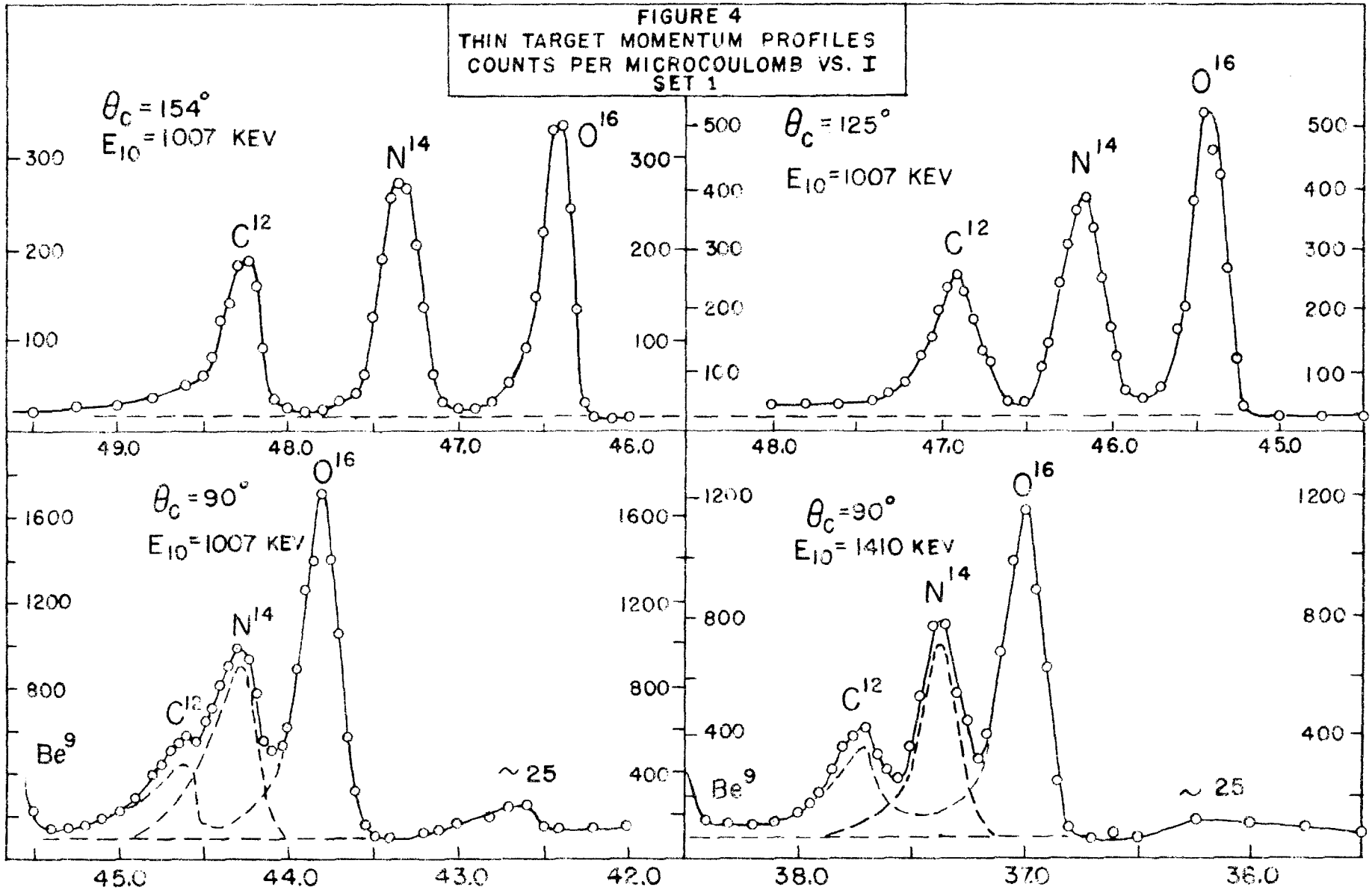

FIGURE 4
THIN TARGET MOMENTUM PROFILES
COUNTS PER MICROCOULOMB VS. I
SET 1

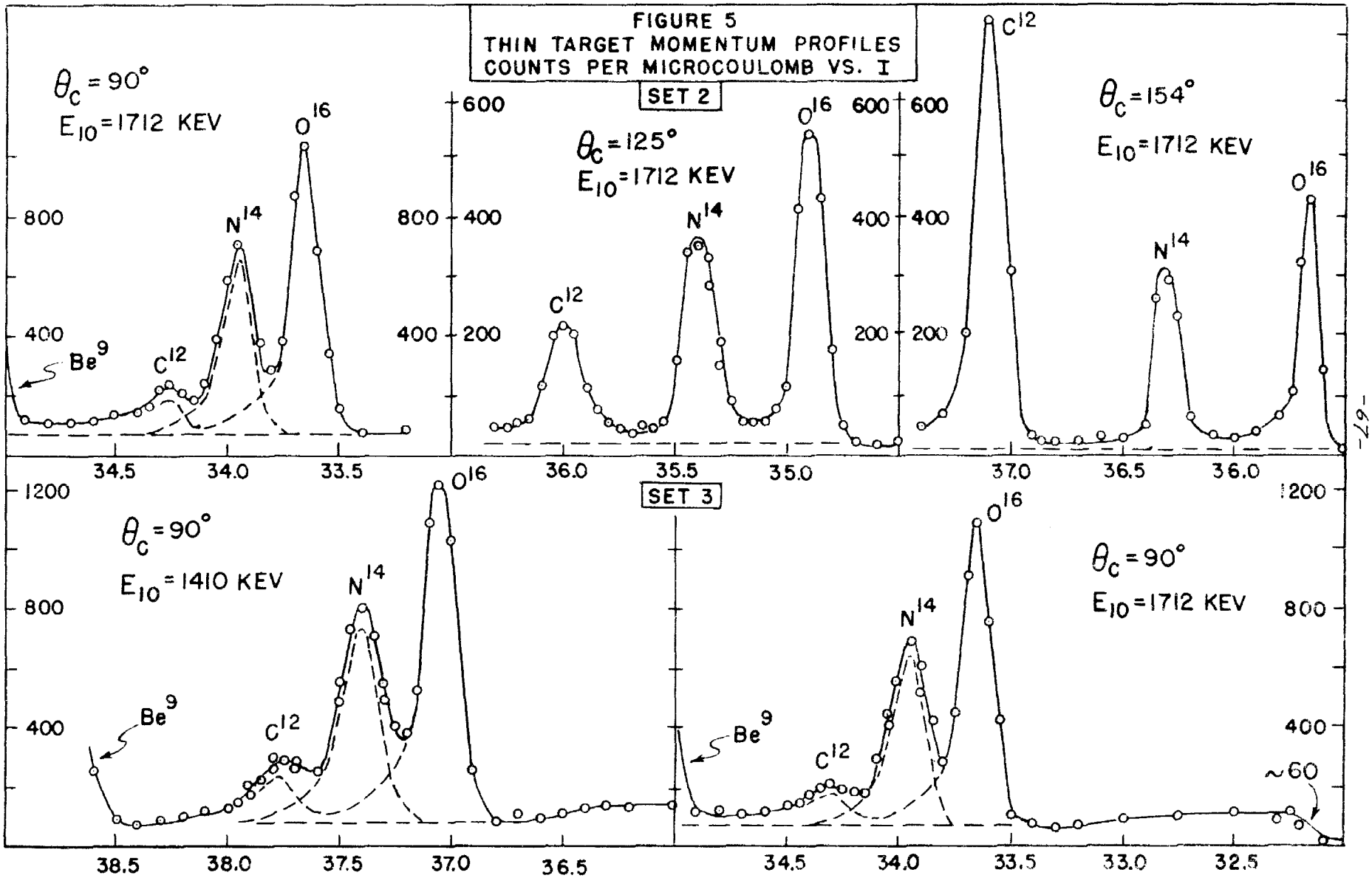
FIGURE 5
THIN TARGET MOMENTUM PROFILES
COUNTS PER MICROCOULOMB VS. I
SET 2
SET 3
θc = 90°
E10 = 1712 KEV
θc = 125°
E10 = 1712 KEV
θc = 154°
E10 = 1712 KEV
θc = 90°
E10 = 1410 KEV
θc = 90°
E10 = 1712 KEV
Be9
C12
N14
O16
~60
800
400
600
200
1200
34.5
34.0
33.5
36.0
35.5
35.0
37.0
36.5
38.5
38.0
37.5
33.0
32.5

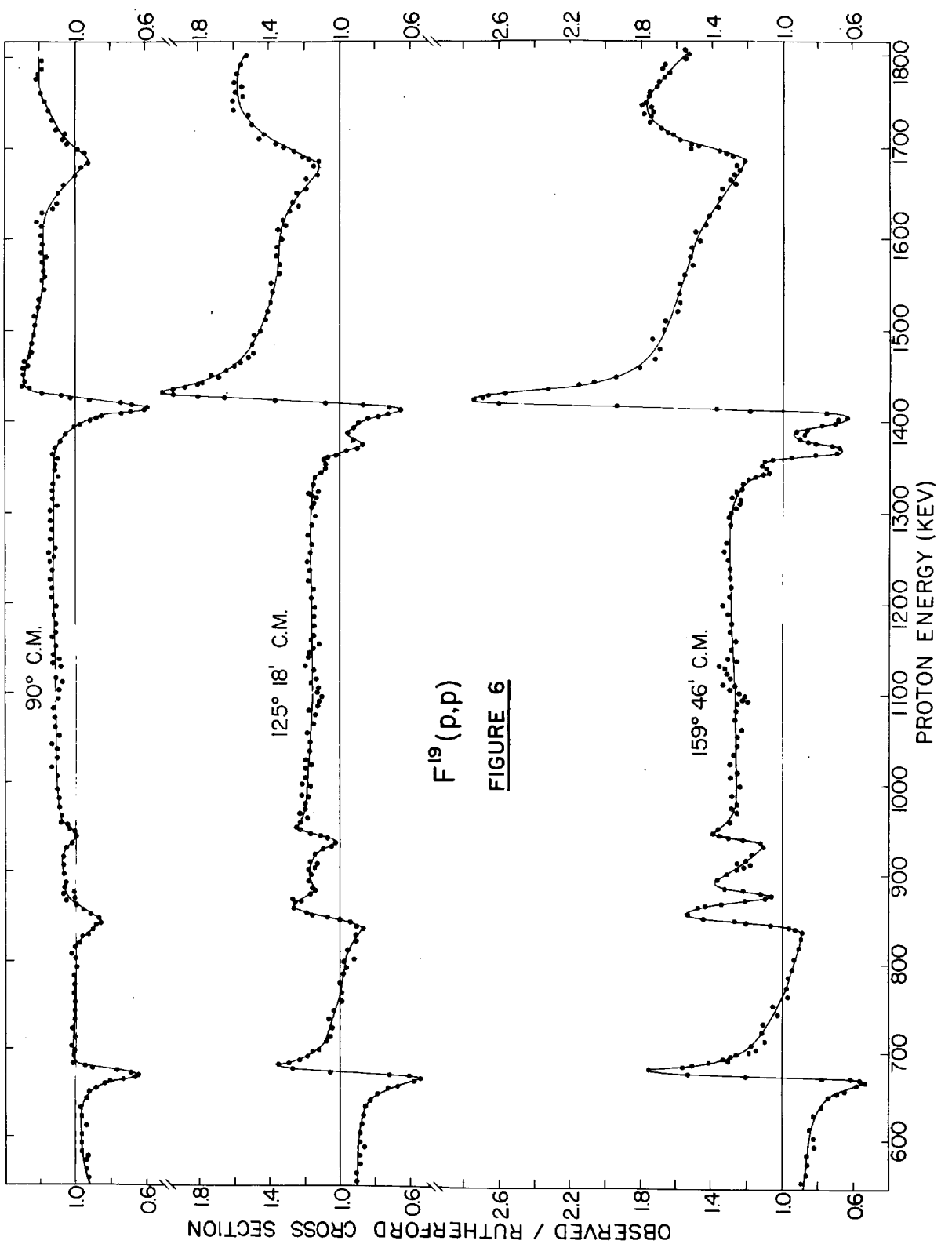
90° C.M.
125° 18' C.M.
159° 46' C.M.
F19(p,p)
OBSERVED / RUTHERFORD CROSS SECTION
PROTON ENERGY (KEV)
1.0
0.6
1.8
1.4
2.6
2.2
600
700
800
900
1000
1100
1200
1300
1400
1500
1600
1700
1800

FIGURE 6

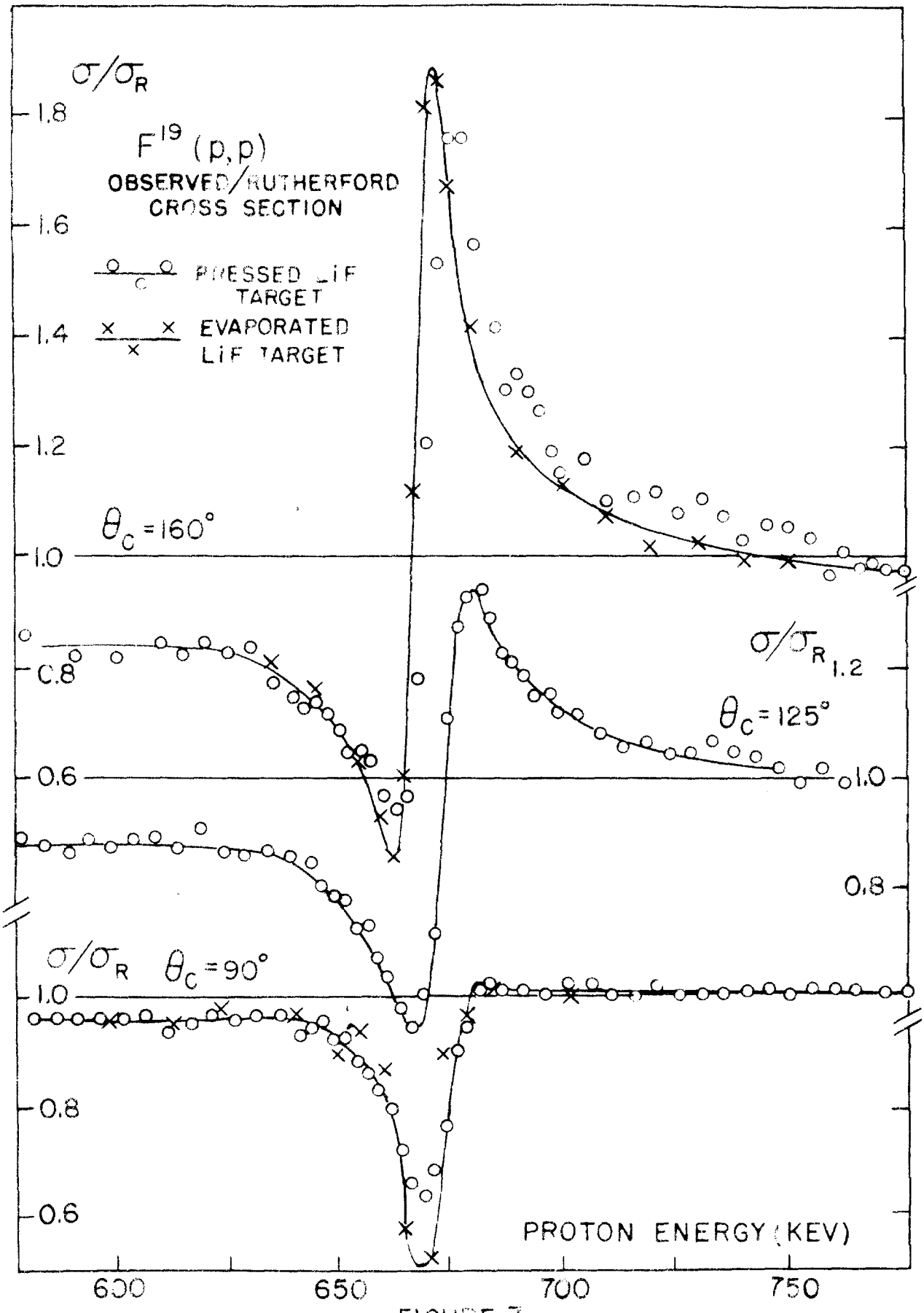
σ/σR
F19 (p,p)
OBSERVED/RUTHERFORD
CROSS SECTION
PRESSED LiF
TARGET
EVAPORATED
LiF TARGET
θc = 160°
σ/σR 1.2
θc = 125°
σ/σR θc = 90°
PROTON ENERGY (KEV)
1.8
1.6
1.4
1.2
1.0
0.8
0.6
600
650
700
750

FIGURE 7

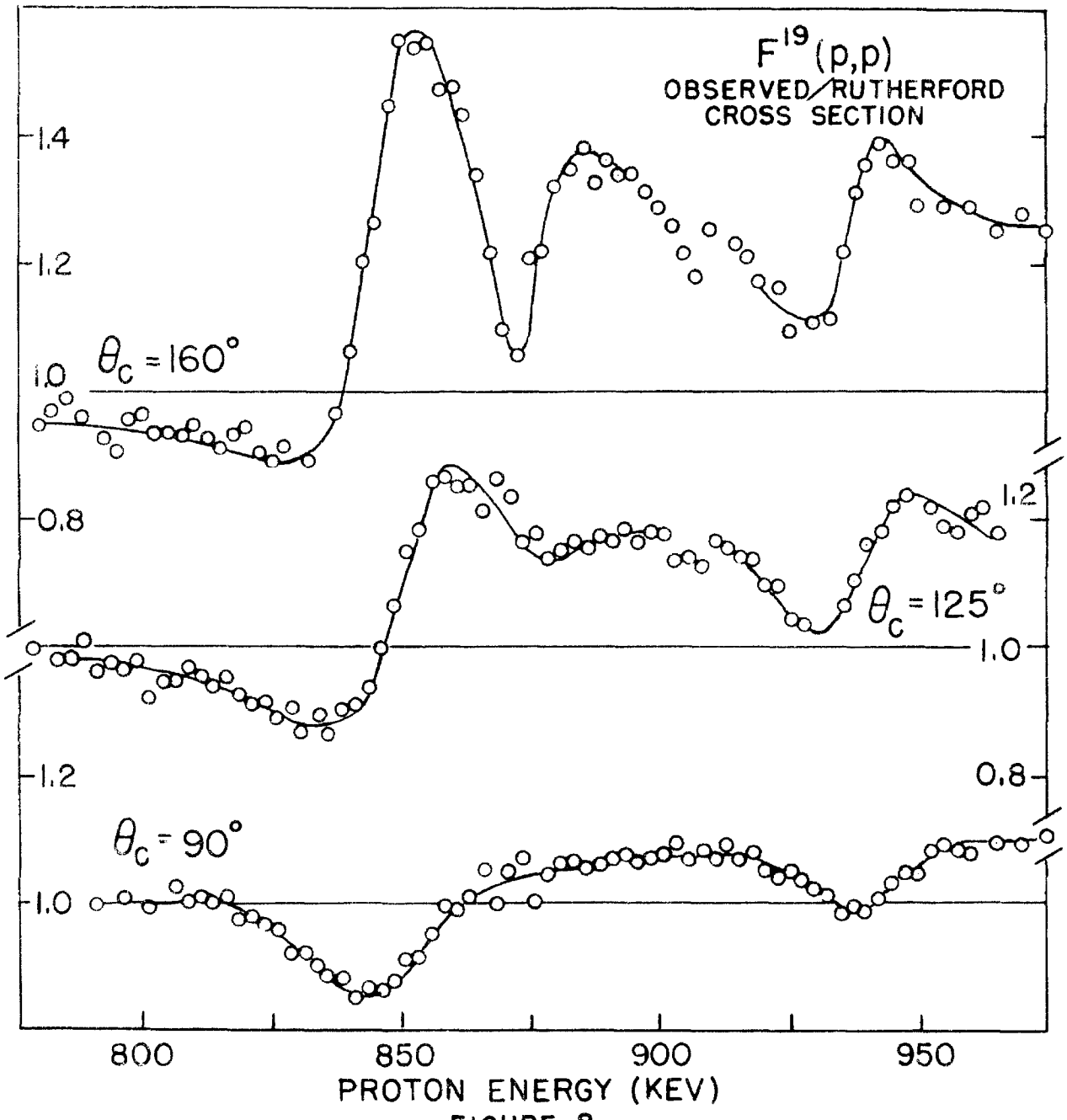
$F^{19}(p,p)$
OBSERVED/RUTHERFORD
CROSS SECTION
1.4
1.2
1.0
$\theta_c = 160°$
0.8
1.2
$\theta_c = 125°$
1.0
1.2
0.8
$\theta_c = 90°$
1.0
800
850
900
950
PROTON ENERGY (KEV)

FIGURE 8

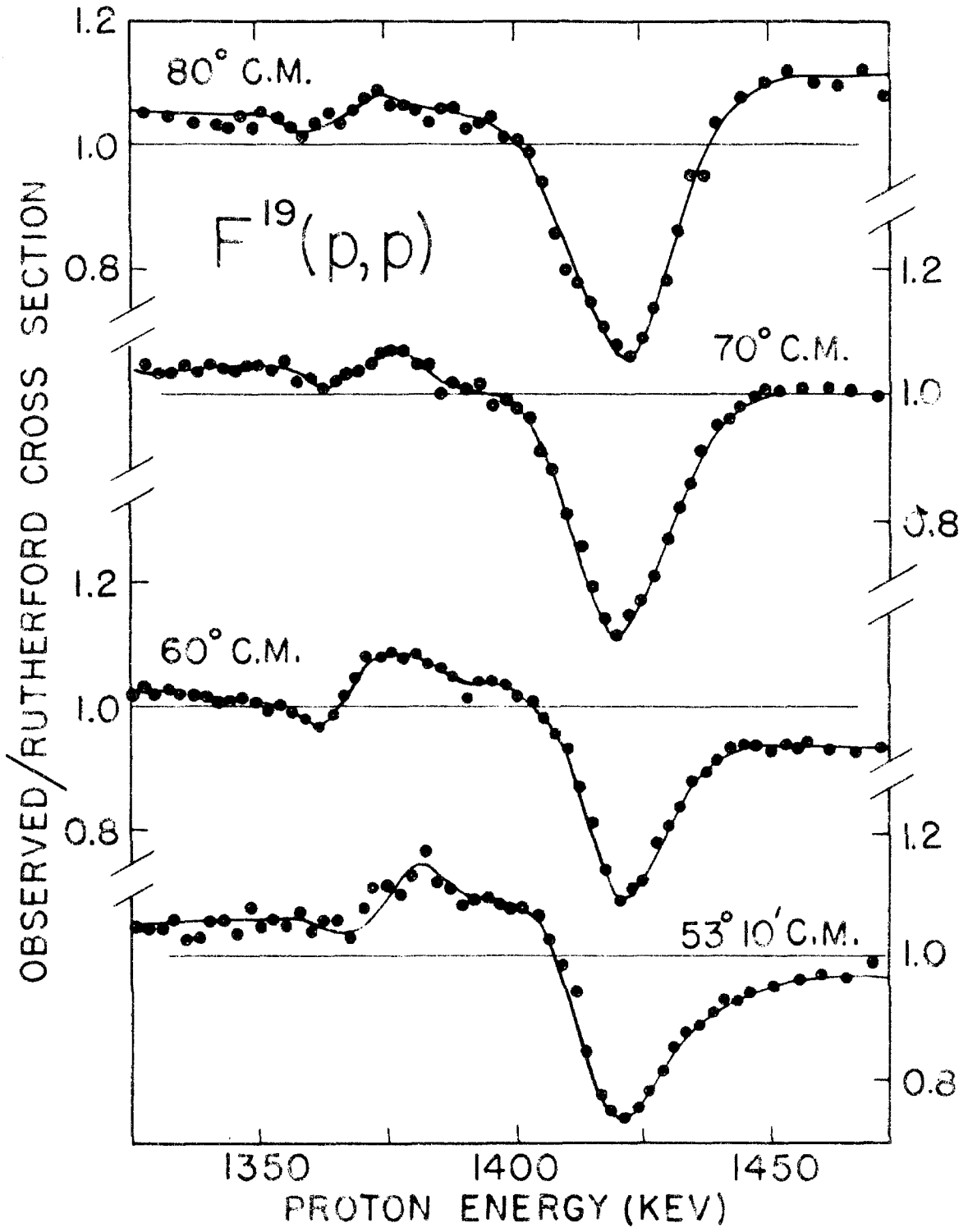
80° C.M.
F19(p,p)
70° C.M.
60° C.M.
53° 10′ C.M.
1.2
1.0
0.8
OBSERVED/RUTHERFORD CROSS SECTION
1350
1400
1450
PROTON ENERGY (KEV)

FIGURE 9

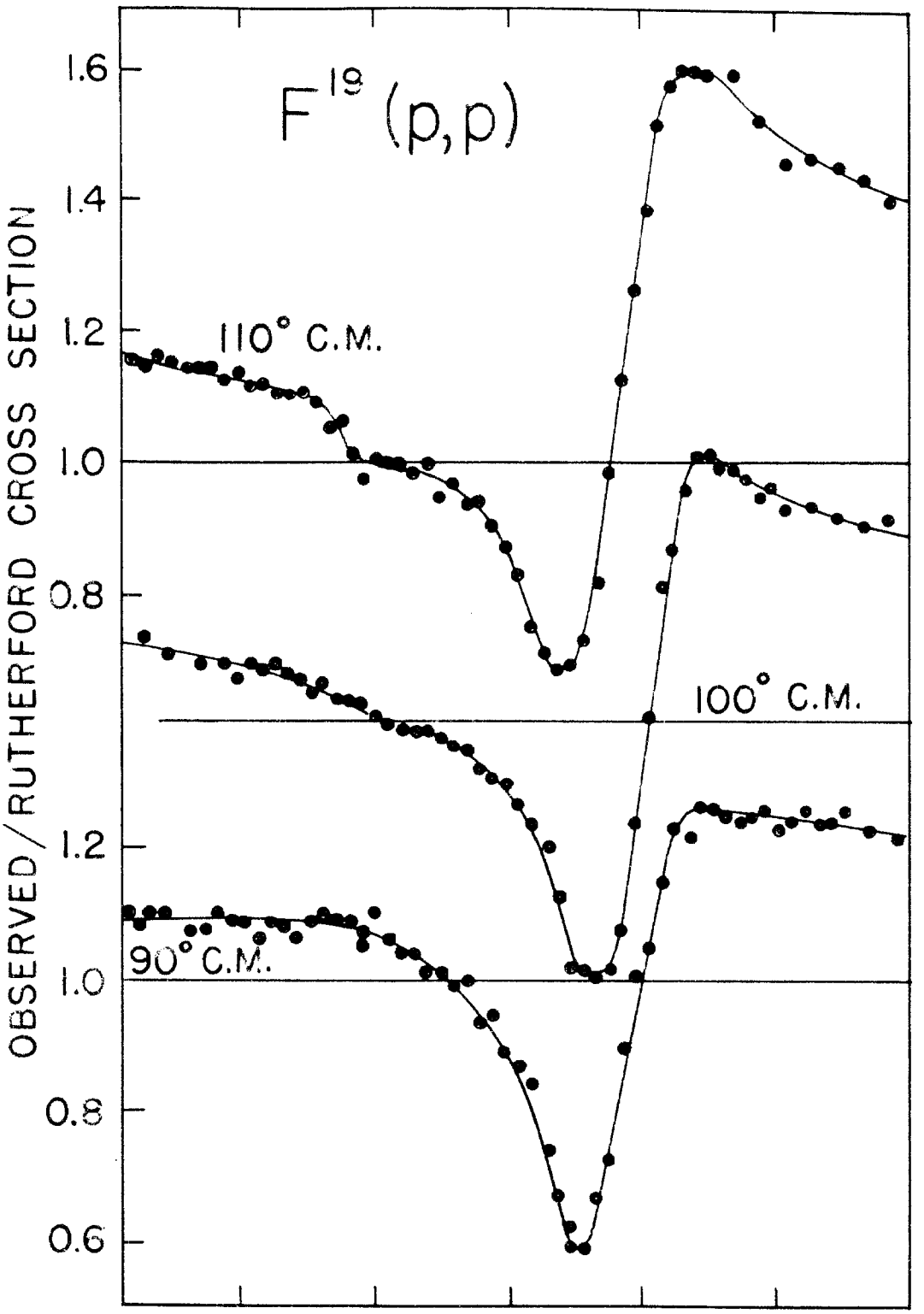
F19 (p,p)
110° C.M.
100° C.M.
90° C.M.
OBSERVED/RUTHERFORD CROSS SECTION
1.6
1.4
1.2
1.0
0.8
1.2
1.0
0.8
0.6
1350
1400
1450
PROTON ENERGY (KEV)

FIGURE 10

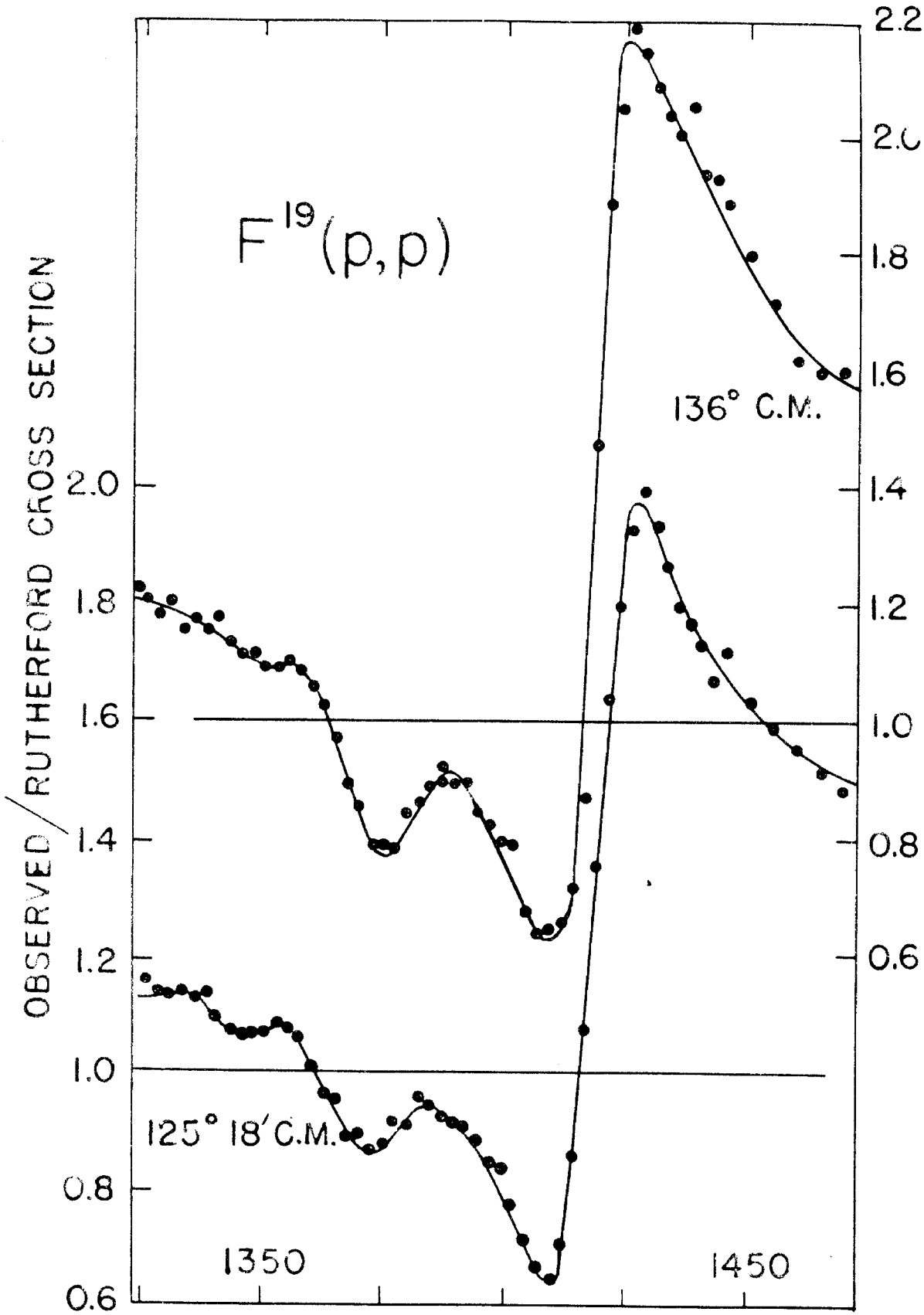
F19(p,p)
136° C.M.
125° 18' C.M.
OBSERVED/RUTHERFORD CROSS SECTION
PROTON ENERGY (KEV)
1350
1450
2.2
2.0
1.8
1.6
1.4
1.2
1.0
0.8
0.6

FIGURE II

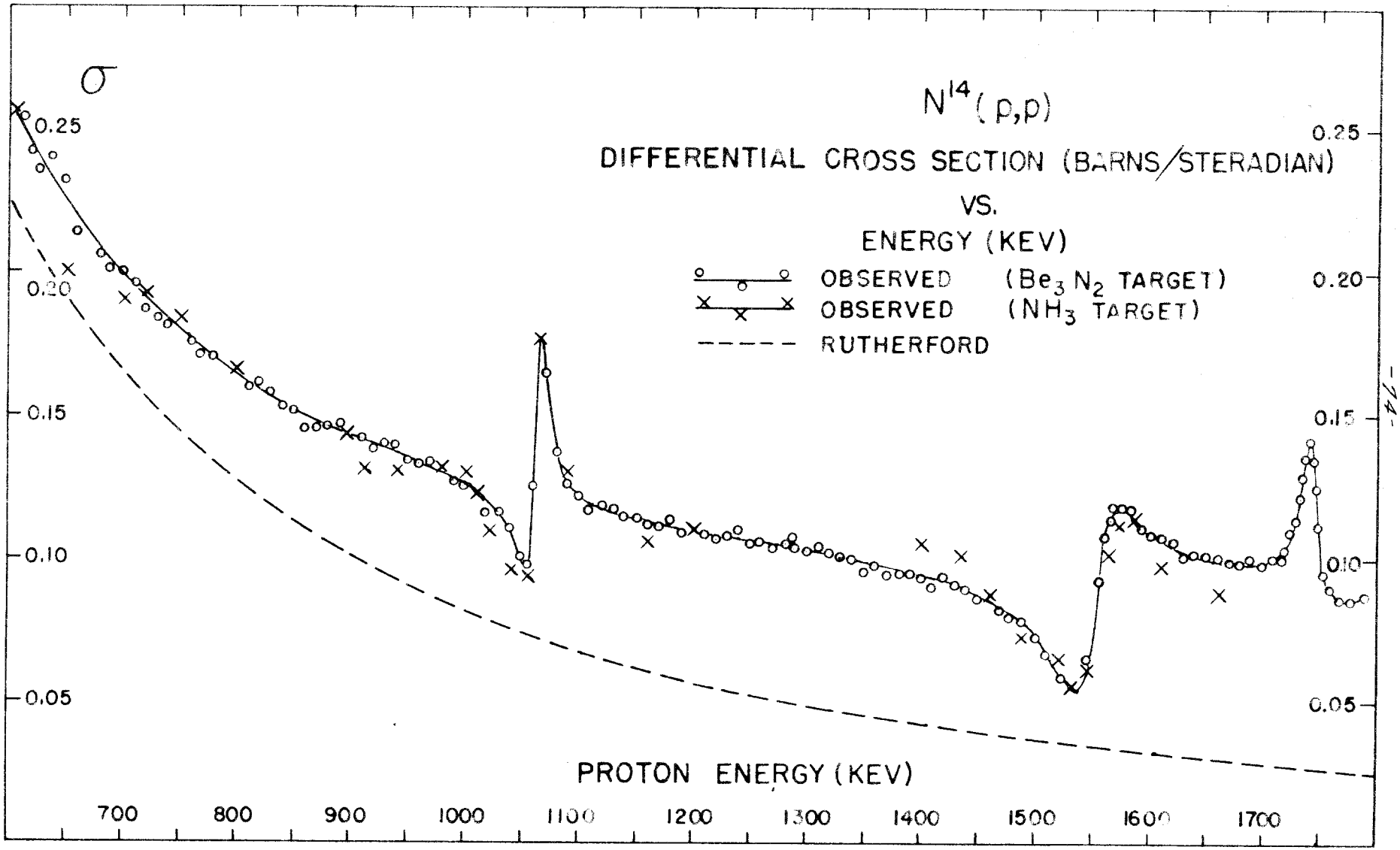
σ
$N^{14}(p,p)$
DIFFERENTIAL CROSS SECTION (BARNS/STERADIAN)
VS.
ENERGY (KEV)
OBSERVED (Be_3N_2 TARGET)
OBSERVED (NH_3 TARGET)
RUTHERFORD
0.25
0.20
0.15
0.10
0.05
PROTON ENERGY (KEV)
700
800
900
1000
1100
1200
1300
1400
1500
1600
1700

FIGURE 12

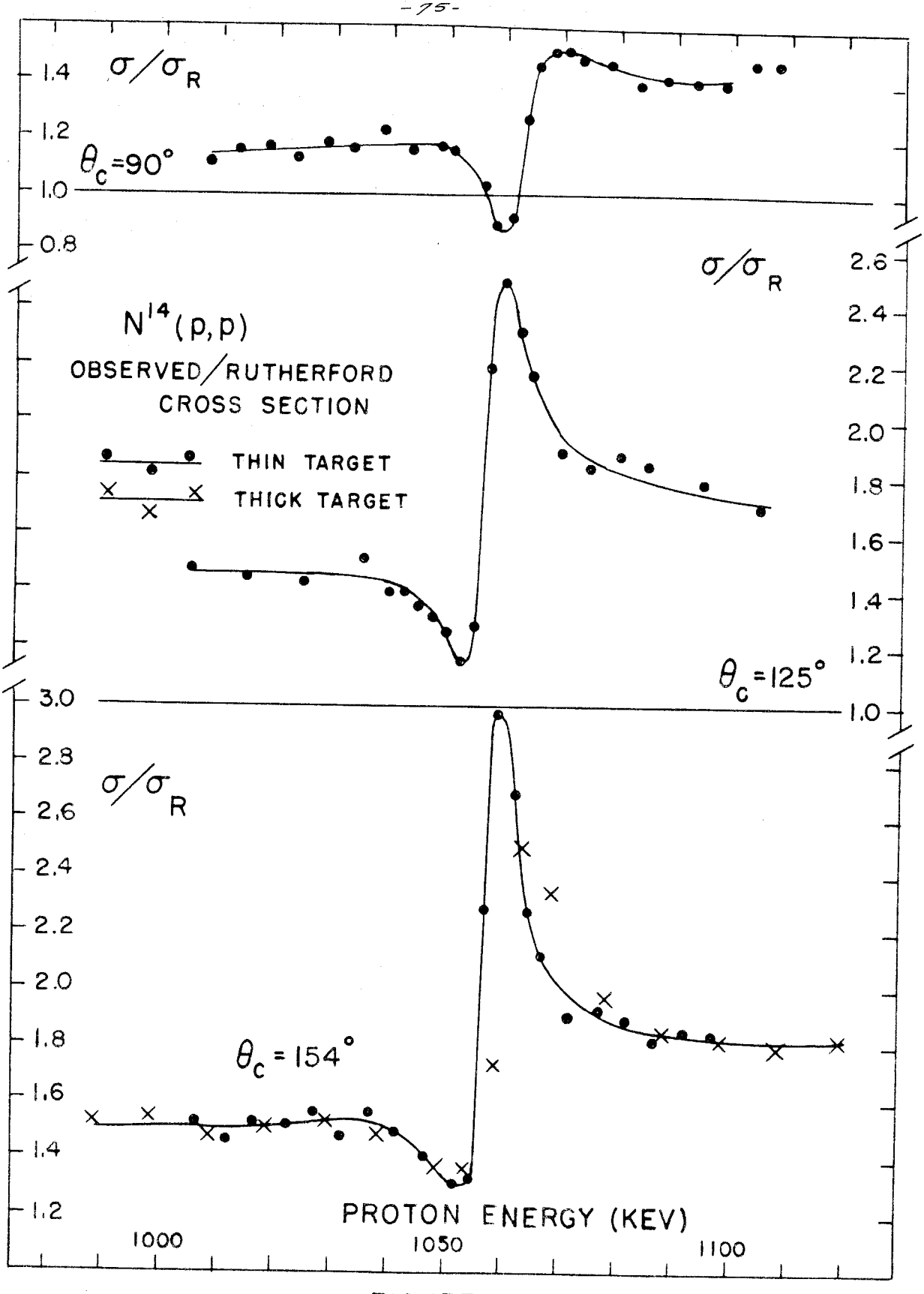
σ/σR
θc=90°
1.4
1.2
1.0
0.8
N14(p,p)
OBSERVED/RUTHERFORD
CROSS SECTION
THIN TARGET
THICK TARGET
σ/σR
θc=125°
2.6
2.4
2.2
2.0
1.8
1.6
1.4
1.2
1.0
3.0
2.8
2.6
2.4
2.2
2.0
1.8
1.6
1.4
1.2
σ/σR
θc = 154°
PROTON ENERGY (KEV)
1000
1050
1100

FIGURE 13

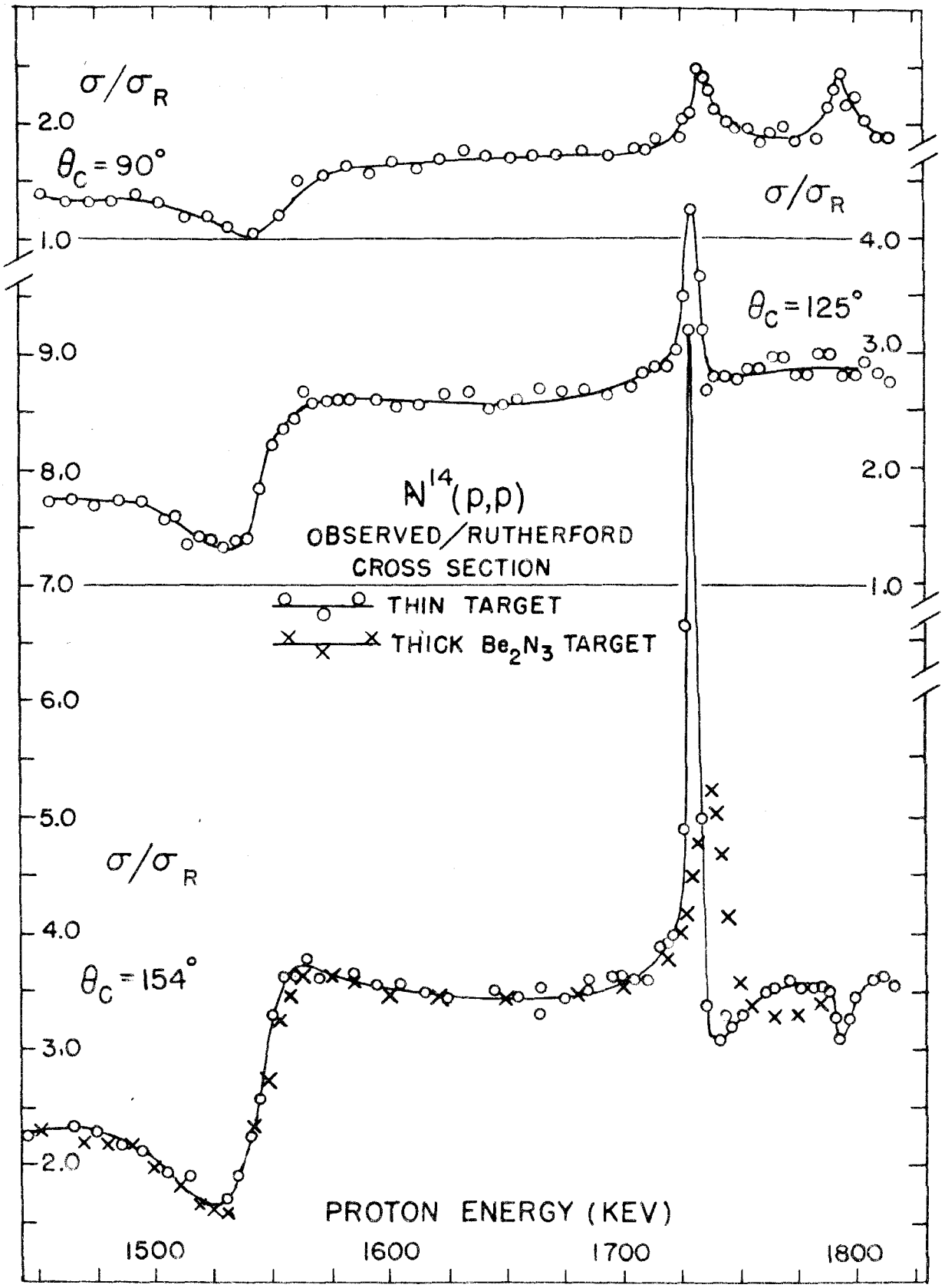
σ/σR
2.0
θc = 90°
1.0
σ/σR
4.0
θc = 125°
9.0
3.0
8.0
2.0
N14(p,p)
OBSERVED/RUTHERFORD
CROSS SECTION
7.0
1.0
THIN TARGET
THICK Be2N3 TARGET
6.0
5.0
σ/σR
4.0
θc = 154°
3.0
2.0
PROTON ENERGY (KEV)
1500
1600
1700
1800

FIGURE 14

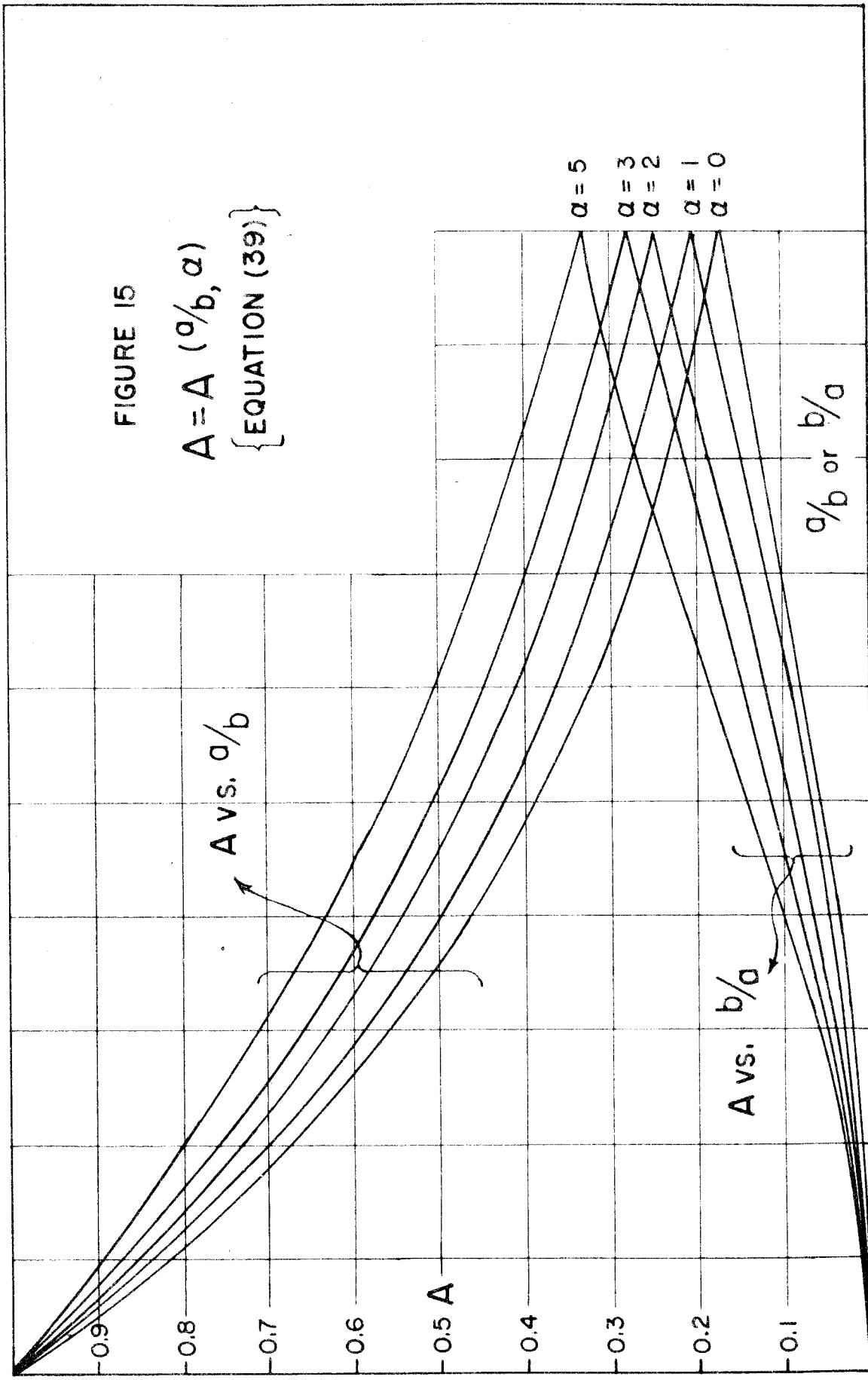
FIGURE 15
A = A (a/b, α)
{EQUATION (39)}
α = 5
α = 3
α = 2
α = 1
α = 0
A vs. a/b
A vs. b/a
A
a/b or b/a
0.1
0.2
0.3
0.4
0.5
0.6
0.7
0.8
0.9
1.0

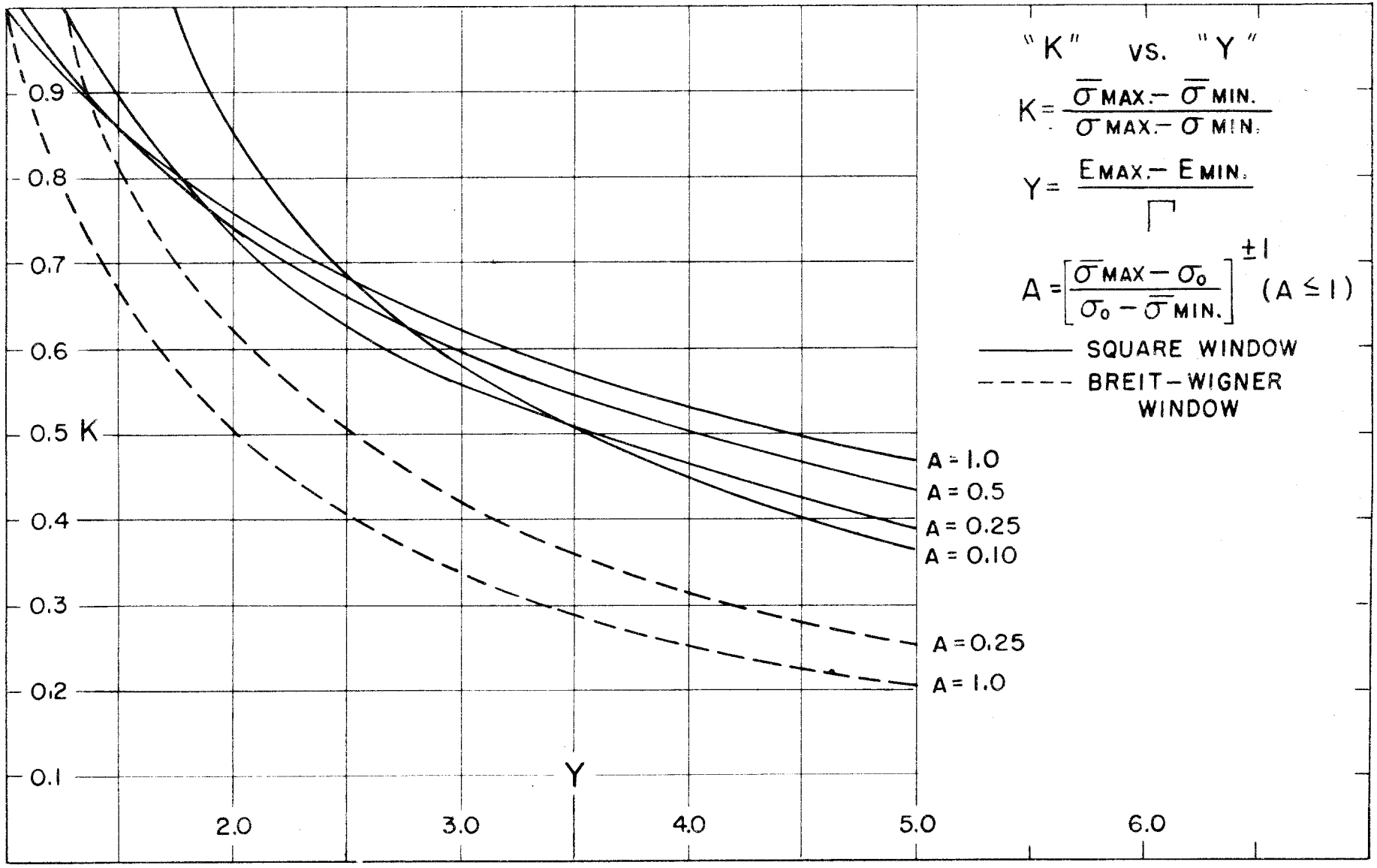
"K" VS. "Y"
$K = \frac{\bar{\sigma}_{MAX.} - \bar{\sigma}_{MIN.}}{\sigma_{MAX.} - \sigma_{MIN.}}$
$Y = \frac{E_{MAX.} - E_{MIN.}}{\Gamma}$
$A = \left[\frac{\bar{\sigma}_{MAX} - \sigma_0}{\sigma_0 - \bar{\sigma}_{MIN.}}\right]^{\pm 1}$ $(A \leq 1)$
SQUARE WINDOW
BREIT-WIGNER WINDOW
A = 1.0
A = 0.5
A = 0.25
A = 0.10
A = 0.25
A = 1.0
K
Y
0.9
0.8
0.7
0.6
0.5
0.4
0.3
0.2
0.1
2.0
3.0
4.0
5.0
6.0

FIGURE 16

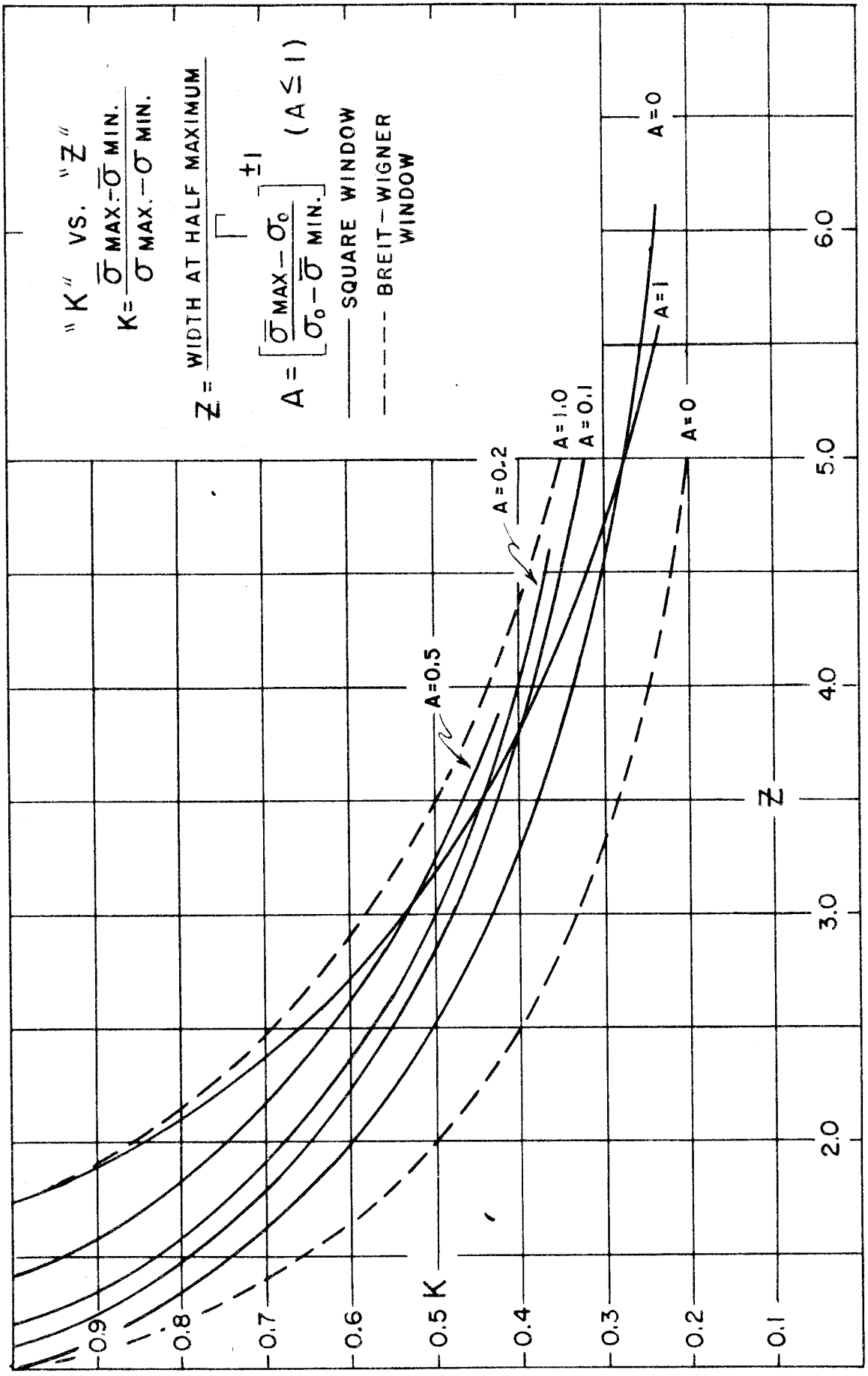
"K" VS. "Z"
$K = \frac{\overline{\sigma}_{MAX.} - \overline{\sigma}_{MIN.}}{\sigma_{MAX.} - \sigma_{MIN.}}$
$Z = \frac{\text{WIDTH AT HALF MAXIMUM}}{\Gamma}$
$A = \left[\frac{\overline{\sigma}_{MAX} - \sigma_0}{\sigma_0 - \overline{\sigma}_{MIN.}}\right]^{\pm 1}$ (A ≤ 1)
SQUARE WINDOW
BREIT-WIGNER WINDOW
A=0
A=1
A=0
A=1.0
A=0.1
A=0.2
A=0.5
K
Z
0.9
0.8
0.7
0.6
0.5
0.4
0.3
0.2
0.1
2.0
3.0
4.0
5.0
6.0

FIGURE 17

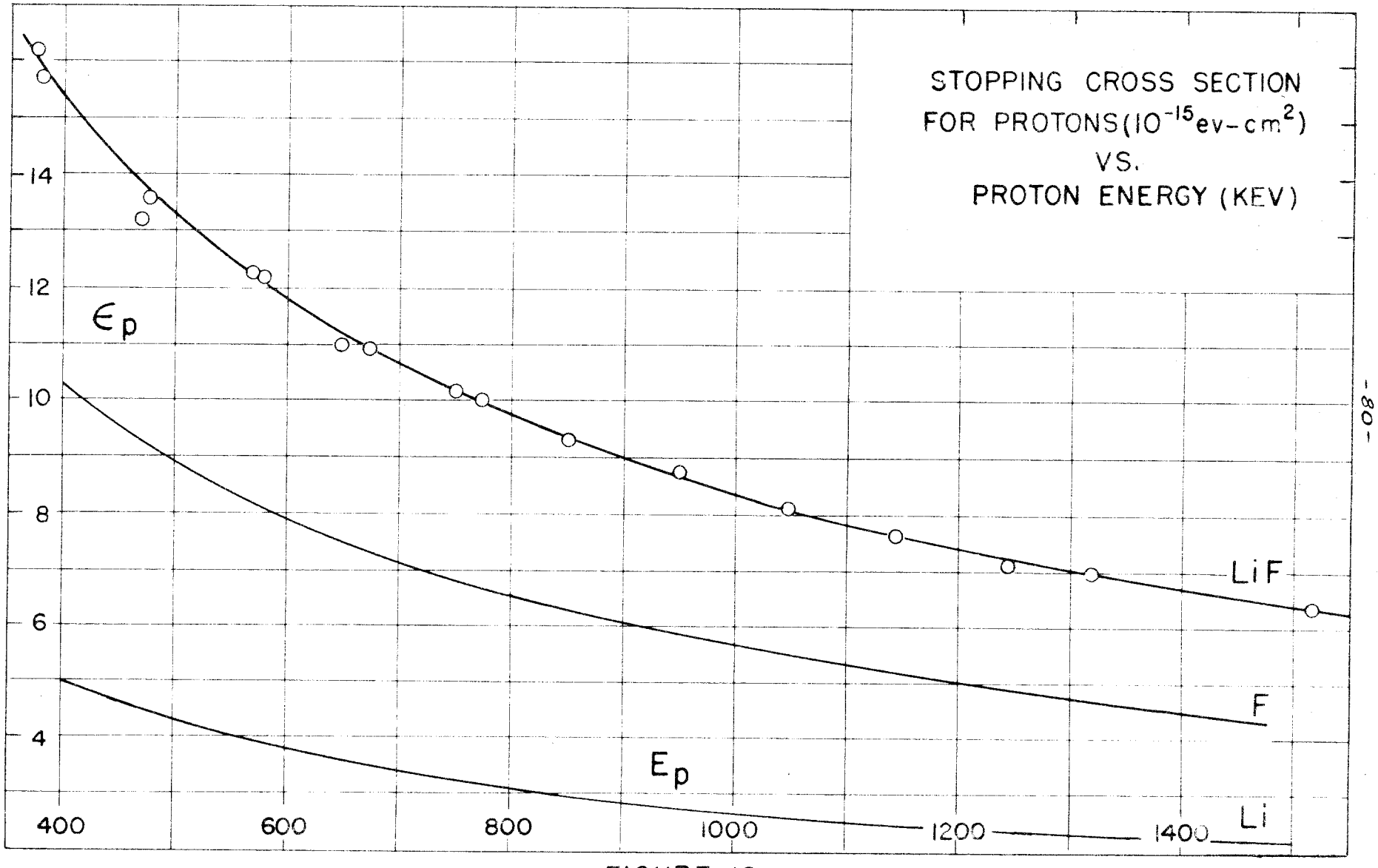
STOPPING CROSS SECTION
FOR PROTONS(10^{-15}ev-cm^2)
VS.
PROTON ENERGY (KEV)
ϵ_p
E_p
LiF
F
Li
14
12
10
8
6
4
400
600
800
1000
1200
1400

FIGURE 18